Article

Selective Copper Complex-catalyzed Hydrodefluorination of Fluoroalkenes and Allyl Fluorides: A Tale of Two Mechanisms

Nicholas O. Andrella, Nancy Xu, Bulat M. Gabidullin, Christian Ehm, and R. Tom Baker

J. Am. Chem. Soc., **Just Accepted Manuscript** • DOI: 10.1021/jacs.9b03101 • Publication Date (Web): 17 Jun 2019

Selective Copper Complex-catalyzed Hydrodefluorination of Fluoroalkenes and Allyl Fluorides: A Tale of Two Mechanisms.

Nicholas O. Andrella[1], Nancy Xu[1], Bulat M. Gabidullin[1], Christian Ehm*[2], and R. Tom Baker*[1]

[1] Department of Chemistry and Biomolecular Sciences and Centre for Catalysis Research and Innovation, 30 Marie Curie, University of Ottawa, ON K1N 6N5 Canada

[2] Università di Napoli Federico II, Dipartimento di Scienze Chimiche, Via Cintia 80126 Napoli, Italy

KEYWORDS. Hydrodefluorination catalysis, Fluoroalkene, Copper, Computational mechanistic study, Ligand-induced mechanism changes

ABSTRACT: The transition to more economically friendly small-chain fluorinated groups is leading to a resurgence in the synthesis and reactivity of fluoroalkenes. One versatile method to obtain a variety of commercially relevant hydrofluoroalkenes involves the catalytic hydrodefluorination (HDF) of fluoroalkenes using silanes. In this work it is shown that copper hydride complexes of tertiary phosphorus ligands (L) can be tuned to achieve selective multiple HDF of fluoroalkenes. In one example, HDF of hexafluoropropene dimer affords a single isomer of heptafluoro-2-methylpentene in which five fluorines have been selectively replaced with hydrogens. DFT computational studies suggest distinct HDF mechanisms for L_2CuH (bidentate or bulky monodentate phosphines) and L_3CuH (small cone angle monodentate phosphines) catalysts, allowing for stereocontrol of the HDF of trifluoroethylene.

INTRODUCTION

The synthesis and chemistry of fluorinated alkenes [FAs] is currently experiencing a renaissance[1,2] due to the need for smaller fluorinated chains[3] in materials applications (cf. environmental persistence of long chain fluorocarbons)[3c,d] and the development of economical late-stage fluoroalkylation processes,[2] including cross-metathesis.[4] Moreover, selected unsaturated hydrofluoroalkenes have been identified as low global warming potential refrigerants [e.g. H_2C=$CFCF_3$, R-1234yf] and blowing agents [e.g. (*Z*)-CF_3HC=$CHCF_3$, R-1336mzz(Z)] when compared to their saturated counterparts [i.e. hydrofluorocarbon refrigerants and blowing agents, such as R-134a, R-401a, R-245fa, etc.].[5] Most currently used synthetic routes to the latter employ well-established technologies (i.e. halogen exchange [Swarts fluorination], HX elimination [X = halogen]) that require harsh/caustic conditions, HF and expensive reactors.[5] Catalytic hydrodefluorination [HDF] represents a potential alternative.[6] Selective and potentially consecutive C-F bond activation and substitution by C-H bonds, could provide new routes to these valuable compounds and additional previously unavailable FAs.

Detailed studies of metal-catalyzed HDF have been focused largely on fluoroarenes but these reaction conditions are not easily transposed to FAs, as their mechanisms can be quite different. For example, fluoroarene HDFs generally proceed by attack of the hydride at the Cα-F carbon (**Scheme 1a,b**) while FAs typically undergo hydride attack at the Cβ-CF carbon (**Scheme 1c,d**).[7] To further complicate matters, the addition of M-H to the FA can proceed either via the more traditional insertion mechanism (**Scheme 1c**) or, as is shown herein, by nucleophilic addition of the hydride generating an intimate ion pair (**Scheme 1d**). It can be expected that the disparity between the activation energies of these processes could lead to significantly different outcomes, especially when considering product distribution in a multi HDF reaction.

Furthermore, selectivity issues with HDF of fluoroarenes are less problematic because as fluorine is removed, HDF becomes more difficult. On top of this, the use of directing groups can increase selectivity. However, such strategies are not necessarily available when using FAs as substrates.[8] Product selectivity must arise from the inherent reactivity of the catalyst or rely on thermodynamic distribution of isomers with the former often leading to uncontrolled multi-HDF and the latter leaving little control for obtaining the desired product.

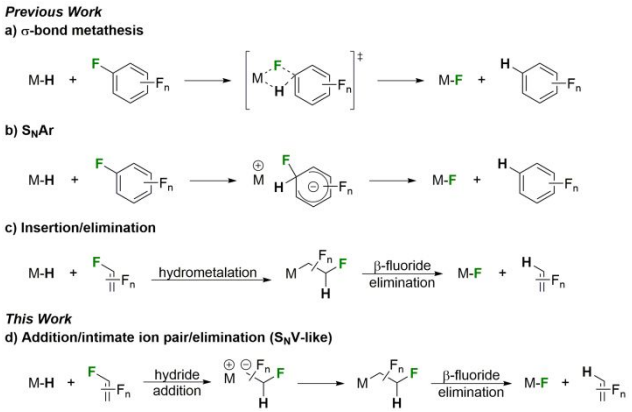

Scheme 1. HDF of fluoroarenes *vs* fluoroalkenes.

In studies of HDF of hexafluoropropene (HFP, **1a**; **Scheme 2**), Jones *et al.* reported the use of stoichiometric zirconocene dihydride for consecutive substitution but selectivity could

only be achieved with careful control of the Zr/FA stoichiometry.[9] Similarly, using a stoichiometric ruthenium hydride complex, Whittlesey and co-workers converted **1a** to a 5:3 mixture of mono- and dihydrodefluorinated products.[10] Holland *et al.* demonstrated the iron complex-catalyzed HDF of FAs although turnover numbers (ToNs) were limited and high temperature was required (100 °C).[11] In contrast, Lentz and co-workers showed that Ti-based catalysts are active under ambient conditions with ToN up to 125 although dihydrodefluorination was only observed in trace amounts.[12] Another contribution from the Lentz group showed that HDF of FAs using Al or Ga hydrides can be catalyzed by N- and O-donors with ToNs up to 87.[13]

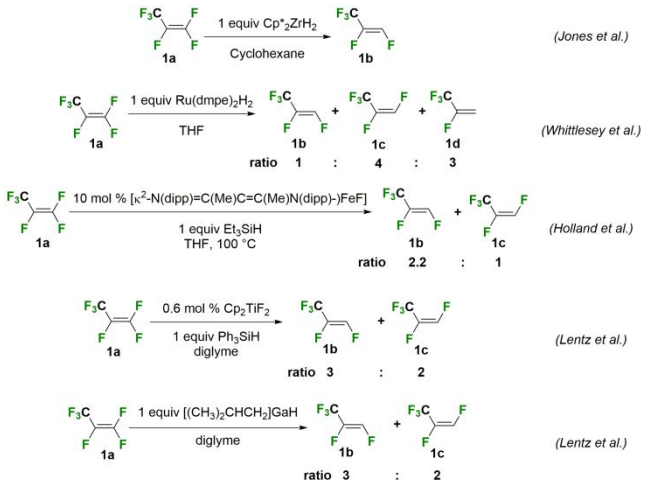

Scheme 2. Some examples of the HDF of hexafluoropropene

Recent studies have identified the potential of copper complexes for catalyzed HDF of FAs (**Scheme 3**).[14] For example, the groups of Shi and of Ito have reported the HDF of *gem*-difluoroalkenes to *E*- and *Z*-terminal monofluoroalkenes with high stereoselectivity using copper(I) catalysts and base. Building on this body of knowledge, we recently reported that isolated phosphine copper hydride complexes readily insert HFP, followed by rapid ß-fluoride elimination to yield Cu-F and 1,2,3,3,3-pentafluoropropene (PFP, **1b,1c**).[14c] Using a similar methodology employing silanes to regenerate Cu-H from Cu-F, a catalytic HDF could be established (**Scheme 3**).[14d]

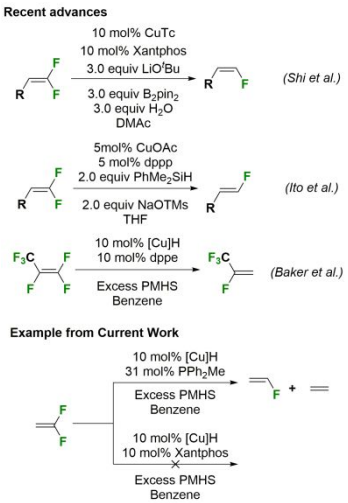

Scheme 3. Copper complex-catalyzed HDF of fluoroalkenes. [PMHS = polymethylhydrosiloxane]

As such, described herein is the reactivity of P-ligated [Cu]-H with various FAs, development of tunable selectivity in Cu complex-catalyzed HDF, and discovery of a new catalytic HDF pathway. The latter allows for stereocontrol with some FAs and for the HDF of less electrophilic FAs, like vinylidene difluoride (**2e**) (**Scheme 3, bottom**).

RESULTS AND DISCUSSION

Catalyzed HDF Reactions. *Ligand Screening.* Extending our previous work to include catalytic HDF, excess dimethylphenyl silane (vs **1a**) was added to the reaction of a catalytic amount of $[CuH(PPh_3)]_6$ (10 mol % Cu) with **1a** at 45 °C for 8 h. Heating the reaction at 45 °C provided the optimal rate, as higher temperatures were found to decompose the catalyst (reactions turned brown) or lead to HFP oligomerization[14c]. As expected, this reaction led readily a mixture of *E*- and *Z*-1,2,3,3,3-pentafluoropropene isomers (PFP, **1b,c**) but, unexpectedly, also 2,3,3,3-tetrafluoropropene (**1d**), in a rare double HDF (**Table 1, Entry 1**). It is notable that substitution of (*E*)-PFP, **1b**, is significantly favored vs the *Z*-isomer, **1c**, such that **1b** has been entirely consumed while **1c** still remains. No additional HDF was observed after another 24 h. No differences in reactivity were observed when employing less expensive tetramethyldisiloxane (TMDS) (**Table 1, Entry 2**) or even moisture-tolerant waste product polymethylhydrosiloxane (PMHS) (**Table 1**, **Entry 3**). Similarly, the change in solvent had little impact on the reaction outcome, except for dimethylformamide (DMF), which gave the same product ratios independent of ligand, followed by rapid catalyst deactivation (See SI Table S1). However, while toluene and tetrahydrofuran (THF) both worked well on NMR scale, they failed to match benzene for consistent results when scaled to 1 L of HFP. Monitoring the conversion of **1a** by ^{19}F NMR spectroscopy showed that addition of 3 equiv. or even excess PPh_3 gave no change in the HDF product slate (**Table 1, Entries 4,5**).

In contrast, the HDF product distribution showed a pronounced ligand effect (

Table 1). When employing bulky electron-rich ligands, like tBuXphos or PCy_3 (**Table 1, Entries 7,8**), similar product ratios to that with no added ligand were observed. Using the bulky aromatic phosphine, P(*o*-tolyl)$_3$, however, the reaction converted HFP to **1b/c** isomers and then quickly ceased to be functional (**Table 1, Entry 6**). This was based qualitatively on a color change from orange to green and, quantitatively, upon addition of more HFP that failed to react. For **1a**, bidentate ligands generated more efficient HDF catalysts. Bis(phosphines) dppe, dppf and Xantphos (**Table 1**, **Entries 9-11**) all readily converted **1a** to **1d** and even 1,1-difluoropropene, **1f**, although the latter likely arises from HDF of 1,1,2-trifluoropropene, **1e**. While dppe provided the highest selectivity for **1d**, Xantphos produced **1f** more slowly than dppf. Interestingly, π-acidic triethylphosphite [P(OEt)$_3$] (**Table 1**, **Entry 12**) gave selective tetra-substitution, yielding primarily **1f** in nearly the same amount as dppf. This increased efficiency of the P(OEt)$_3$/CuH catalytic mixture is contrary to the expected activity increase with hydricity using the more σ-donating phosphines, dppf and Xantphos. Both P(OPh)$_3$ and P(O-*o*-tolyl)$_3$ showed significantly reduced reactivity (**Table**

1, Entries 13 and **14**), however, suggesting that ligand size is also an important factor.

Table 1. Ratios of hexafluoropropene HDF products.

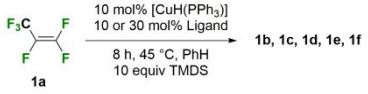

Entry	Ligand	1b/1c	1d	1e	1f
1	None[a]	1[e]	1.7		
2	None	1[e]	1.7		
3	None[b]	1[e]	1.6		
4	PPh_3	1[e]	1.5		
5	PPh_3[c]	1[e]	1.5		
6	P(*o*-tolyl)$_3$	9.5	1		
7	*t*BuXphos	1[e]	1.2		
8	PCy_3	1[e]	1.3		
9	dppe		11		1
10	dppf		1		3.0
11	Xantphos	1	2.4		
12	$P(OEt)_3$			1	2.4
13	$P(OPh)_3$[d]	1			
14	P(O-*o*-tolyl)$_3$	35	1		

Ratios are based on ^{19}F NMR integration of products vs internal standard. All reactions gave 100% conversion of HFP (**1a**) unless indicated otherwise. Following the reaction, the headspace of the reaction was sampled to confirm solution product distribution. a) $PhMe_2SiH$ was used in place of TMDS. b) PMHS was used in place of TMDS; *N.B.* PMHS forms a biphasic mixture with benzene. c) 60 mol % of PPh_3. d) complete conversion of HFP not achieved after 8 h. e) only *Z*-isomer **1c** was observed.

Substrate Scope. Using these optimized conditions with dppf or Xantphos, the scope was investigated for the HDF reaction of various perfluorinated substrates (**Scheme 4**). Both chlorotrifluoroethylene (**3a, Eq. 4.1**) and HFP analogue, trifluoromethyl trifluorovinyl ether (**4a, Eq. 4.2**), yielded a 4:1 mixture of *cis*-:*trans*-1,2-difluoroethylene (**2c,d**), respectively. During the first few hours of the latter reaction trifluoromethyl

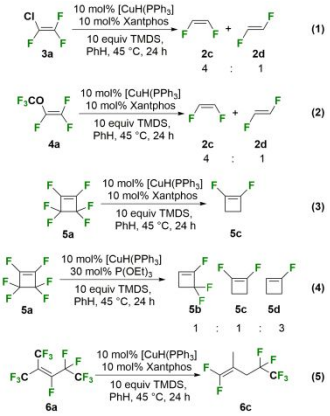

Scheme 4. Selective and multiple HDF of various perfluorinated substrates.

1,2-difluorovinyl ether (**4b**) was observed but then eventually consumed, presumably via β-OCF_3 elimination (**Scheme 5**). Isomer **2c** is presumably formed preferentially due to the *gauche* effect[15] as the *cis* isomer is also the most thermodynamically stable, suggesting a late transition state.

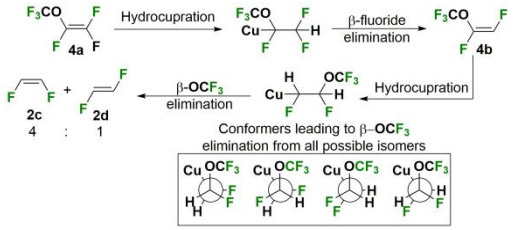

Scheme 5. Top: HDF of **4a** leading to a 4:1 mixture of **2c,d** via β-OCF_3 elimination. **Bottom:** The gauche effect increasing selectivity for **2c**.

The HDF of perfluorocyclobutene (**5a, Eq. 4.3**) and HFP dimer, perfluoro-2-methylpent-2-ene (**6a, Eq. 4.5**) proceeded readily, yielding multi-HDF products. FA **5a** was selectively converted to 1,2-difluorocyclobutene (**5c**) via triple HDF whereas **6a** underwent quintuple HDF to generate the di-alkyl substituted *gem*-difluoroalkene (**6c)**, exclusively. The isomeric HFP dimer, perfluoro-4-methylpent-2-ene (**6b**), also underwent multiple HDF but in an unselective manner, generating multiple products (see SI for details).

Switching to $P(OEt)_3$, the HDF of **5a** produced a mixture of 1,4,4-trifluorofluorocyclobutene (**5b)**, **5c** and 1-fluorocyclobutene (**5d**) in a 1:1:3 ratio before catalyst deactivation (**Eq. 4.4**). As with **1a**, this ligand produced a significantly more active HDF catalyst than the electron-donating bis(phosphines). FA **6a**, as above, yielded only **6c**, demonstrating that this product is too electron-rich to undergo further HDF.

The above electrophilic substrates (i.e. **1a**, **5a**, **6a** and **6b**) did not provide an avenue to test the impact of stronger σ-donating ligands as they react readily with electron-rich phosphines with cone angles smaller than tricyclohexylphosphine (PCy_3).[1g,16] Likewise, the decomposition of CuH complexes containing N-heterocyclic carbenes and nitrogen chelates is well documented,[17] excluding these ligands from consideration. With this in mind, the HDF of less electrophilic trifluoroethylene, **2b**, was performed. Using the optimized reaction conditions and the Xantphos/CuH catalytic mixture, **2b** was readily converted to

cis:*trans* (**2c:2d**) in a 7:1 ratio, reflecting the thermodynamic preference, whereas use of $P(OEt)_3$ gave no reaction (**Scheme 6**). Using three equivalents of basic phosphine $PMePh_2$, however, inverted the **2c:2d** ratio to 1:3.7. As with HFP, hydride addition always occurs regioselectively, suggesting that Cu-H addition to **2b** occurs with the FHC= fragment oriented towards the copper.

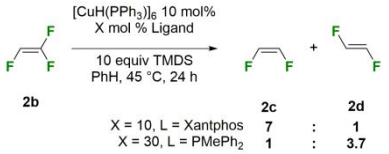

Scheme 6. Ligand-induced inversion of stereoselectivity in HDF of trifluoroethylene.

In contrast to the above substrates, tetrafluoroethylene (**2a**) reacts with the copper hydride complexes to yield thermally stable copper 1,1,2,2-tetrafluoroethyl complexes.[18] As previously reported, addition of a Lewis acid (or base) is required to induce β-fluoride elimination,[2j] presumably via an outer-sphere fluoride-elimination mechanism (**Scheme**).

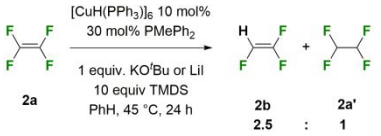

Scheme 7. HDF of **2a** leading to a mixture of **2b**, **2a'** and incomplete conversion of **2a.**

Cu-tetrafluoroethyl complexes. Interestingly, the Cu tetrafluoroethyl complex with $PMePh_2$ can be easily and safely prepared using TFE Safe Supply™ (generated by pyrolysis of potassum perfluoropropionate in vacuo; see experimental). Treatment of Stryker's reagent, 3 equiv. $PMePh_2$ and 1.5 equivalents of tetramethyldisiloxane [TMDS] with **2a**:CO_2 in benzene at 70 °C afforded the Cu-CF_2CF_2H complex $[(PMePh_2)_3Cu(CF_2CF_2H)]$ (**7a**) in good yield (70%) and excellent purity [>90%, **Scheme , Eq. 8.1**]. The use of this methodology with Xantphos or $P(OEt)_3$ did not yield the desired product. The synthesis of the former complex was instead carried out with limonene-inhibited **2a**. In our first attempt, formation of [(Xantphos)Cu(CF_2CF_2H)] (**7b**) was accompanied by the [Cu](CF_2CF_3) analog (**7b'**) derived from insertion of **2a** into [Cu]-F (**Scheme 8, Eq. 8.2**). Addition of 10 % TMDS was sufficient to convert [Cu]-F to [Cu]-H, enabling isolation of pure **7b** in good yield (**Scheme 8, Eq. 8.3**).

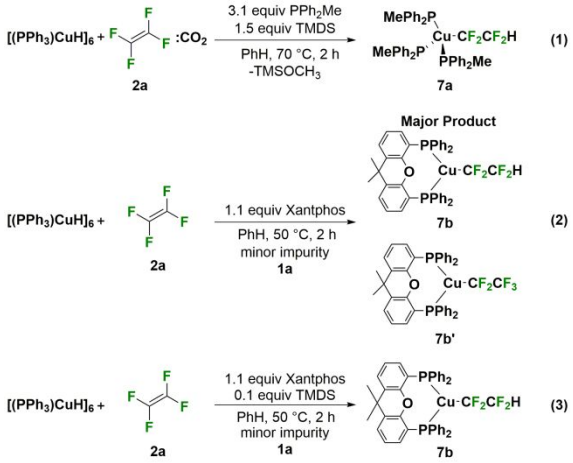

Scheme 8. Synthesis of complexes **7a** and **7b.**

The ^{19}F NMR spectrum of **7a** in C_6D_6 displays two resonances which can be easily differentiated based on their J_{FH} coupling constants: CF_2H = 50 Hz and CF_2R < 1 Hz (unresolved). The ^{31}P NMR spectrum contains a broad singlet at -20.0 ppm and the molecular structure was confirmed by single crystal X-ray diffraction (**Figure 1**).

With three seemingly unrelated observations in hand - a) Using $P(OEt)_3$ in the HDF of HFP (**1a**) generates an active catalyst on par with dppf, b) Using a small cone-angle, strong σ-donating phosphine [$PMePh_2$ vs $P(OEt)_3$] allows for HDF of **2b**; and c) Changing from Xantphos to $PMePh_2$ in the HDF of **2b** inverts isomer ratios of **2c:2d** from 7:1 to 1:3.7 - mechanistic studies and computations were carried out in an attempt to consolidate them.

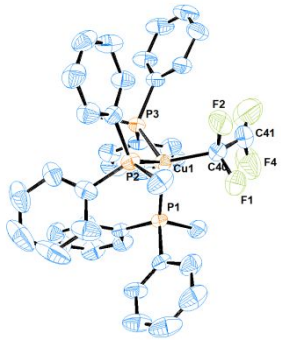

Figure 1. ORTEP representation of the molecular structure of **7a**. Thermal ellipsoid probabilities are set to 35% and hydrogen atoms omitted for clarity.

Mechanistic DFT Studies. To gain deeper insight into the HDF mechanism(s) in these P-ligated copper-hydride systems, we conducted solvent corrected (PCM: benzene) DFT studies at the TPSSh(PCM)/TZ/TPSSTPSS-(PCM)/DZ level of theory. For details and expected accuracy of the method see computational details and supporting information. A model phosphine ligand, L = PMe_3, was chosen to fully analyze possible reaction pathways in the LCu-H, L_2Cu-H and L_3Cu-H systems in the HDF of three prototypical FAs of varying fluorine content, i.e. tetrafluoroethylene (**2a**), trifluoroethylene (**2b**) and 1,1-difluoroethylene (**2e**). Relevant transition states (TS) and resting states (RS) were then analyzed for experimentally employed systems, i.e. L = PPh_3, $PMePh_2$ and

PMe_2Ph, dppe and Xantphos, to understand the pronounced influence of the ligands on the HDF selectivity of **2b**.

*PMe_3 model system. **2a**.* Spectroscopic studies of copper hydrides have shown that the only observable species in solution are dimers,[17a,b,19b-d] unless very bulky ligands are used[19a]. Kinetic studies have indicated that the active species in copper-bis(phosphine)-catalyzed hydrogenation[20] and hydrosilylation[21] reactions are mononuclear. We considered HDF in the present systems to take place in monomeric or dimeric copper systems. For monomeric LCu, L_2Cu and/or L_3Cu system (L = PMe_3), we considered a) an insertion-elimination sequence,[22] b) 'S_NV'-like H-addition as for example observed for early transition metal-catalyzed HDF followed by Cu-C bond formation and subsequent F-elimination[8a] c) single electron transfer,[23,24] d) σ-bond metathesis [4,7e,8a,25-30] or e) 'S_NV'-like H-addition followed by immediate F-elimination.[8a,13c,28] The latter two mechanisms could be quickly excluded; a *σ*-bond metathesis TS could not be located and ion pairs are stable, showing no tendency for immediate F-elimination. SET can be excluded based on the known low electron affinity of (per)fluorinated alkenes.[7e, 8a] An oxidative addition–reductive elimination pathway[8a] can be excluded based on the experimental observation of **7a,b**. Both insertion and H-addition pathways for hydrometallation could be found for monomeric copper systems and H-addition is also possible in a dimeric L_2Cu-(μ-H)$_2$-CuL_2 system.

The $(PMe_3)_2Cu$-(μ-H)$_2$-$Cu(PMe_3)_2$ dimer (-3.7 kcal/mol) is slightly more stable than $(PMe_3)_3Cu$-H (**A**). The first two PMe_3 ligands in $(PMe_3)_3Cu$-H (**A**, 0.0 kcal/mol) are relatively weakly bound (ΔG_{323K} = 7.8 + 5.1 kcal/mol). Nonetheless, this penalty raises the barrier for HDF in the LCu-H system significantly over the corresponding barriers in the L_2 and L_3 systems (see supporting information). Therefore, we will focus the discussion on the competition between L_2 and L_3 HDF pathways. **Figure 2** shows important transition states and **Figure 3** the potential energy surface (PES) for the two competing mechanisms for the example of **2a**.

Hydrometallation in the monomeric L_2 system starts with dissociation of one phosphine ligand from L_3Cu-H (**A**, +7.8 kcal/mol) to form L_2Cu-H (**B**). Thereafter, coordination of **2a** (alkene coord. **TS(B-C)**, +12.6 kcal/mol) forming Cu-olefin complex **C** followed by alkene insertion into the Cu-H bond (HM **TS(C-D)**, +9.1 kcal/mol) represents the lowest energy pathway for HDF to form L_2Cu-CF_2CF_2H (**D**).

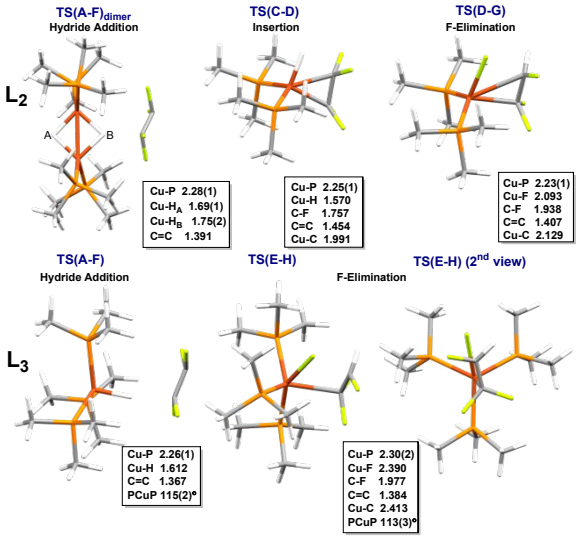

Figure 2. Graphical depiction of important transition states in the HDF system of **2a** with L_3/L_2Cu-H. L = PMe_3. Bond distances in Å, bond angles in deg. Color scheme: C grey, H white, P orange, F lime. Level of theory TPSSTPSS(PCM)/DZ. Solvent = benzene.

The insertion barrier from the Cu-H(alkene) complex **C** is very small (+3.2 kcal/mol) and overall, the coordination **TS(B-C)** is rate-limiting in this process. Nucleophilic H-addition via **TS(B-D)**, although possible in the L_2 system, is associated with a much higher barrier (+17.7 kcal/mol; see discussion of the L_3 system for further details).

Within the monomeric L_2 hydrometallation pathway, alkene coordination is endergonic, but irreversible, as insertion from the alkene complex has a much lower barrier than dissociation of the alkene. That insertion of the FA into the Cu-H bond is associated with only a very small barrier is unsurprising; **TS(C-D)** is geometrically very early compared to the Cu-H(alkene) complex **C** (Cu-H bond length + 0.01 Å, see also **Figure 3**), as coordination to the late TM copper has already activated the C=C double bond and Cu-H bonds are rather weak (~ 60 kcal/mol).[30] Hydrometallation leads to **D** (-38.7 kcal/mol), which can be further stabilized by coordination of another phosphine forming L_3Cu-CF_2CF_2H (-50.4 kcal/mol, **E**).

HDF can also proceed without the release of one phosphine ligand in the L_3 system. Unlike in the monomeric L_2 system, where synchronous hydrometallation via insertion is favored, insertion into the Cu-H bond in the L_3 system proceeds via a two-step, asynchronous, mechanism. Nucleophilic H-addition in this system via **TS(A-F)** has a very low barrier (+7.4 kcal/mol) and proceeds to a contact ion pair (CIP **F**, -17.7 kcal/mol). The low barrier can be understood as a direct result of the destabilization of a C=C double bond by multiple fluorine substituents and the weak Cu-H bond.[31,32] Coordination of a third phosphine stabilizes the forming cation in the TS with respect to the L_2 system. Nucleophilic addition along the Burgi-Dunitz trajectory via **TS(A-F)** is essentially 'dagger-like' and requires minimal space around Cu. Forming a solvent-separated ion pair (SIP, +17.5 kcal/mol) from the CIP is associated with a significant increase in energy (see supporting information). However, full separation is not necessary, as slight reorientation of the anion leads to formation of a Cu-C bond, ultimately yielding L_3Cu-CF_2CF_2H (**E**).

Hydrometallation in the dimeric system proceeds by nucleophilic addition along the Burgi-Dunitz trajectory via **TSA-F$_{dimer}$**, similar to the L_3 system and leads to a similar CIP from which Cu-C bond formation and dimer splitting can proceed via simple reorientation. This pathway is preferred by 4.2 kcal/mol in the model system over the L_3 pathway. The preference stems nearly entirely from the dimer stability (-3.7 kcal/mol) and can be understood, similarly to the L_3 environment, due to the stabilization of a cationic charge. However, unlike the 'dagger-like' L_3 system, the L_2Cu-(μ-H)$_2$-CuL_2 system is much more susceptible to variation of steric bulk in the substrate and the ligands as the phosphine substituents point towards the approaching olefin (see Figure 3).

Insertion of **2a** into the Cu-H bond is irreversible, as the reverse elimination barriers are > 58 kcal/mol. From the resting state **E** (-50.4 kcal/mol), F-elimination can again proceed, after phosphine decoordination, via L_2 **TS(D-G)** (-10.3 kcal/mol) or, interestingly, also directly from the L_3 species (-13.9 kcal/mol) via **TS(E-H)**. The latter one is preferred for formation of **2b**. The lowest F-elimination pathway is still associated with a significant barrier (36.5 kcal/mol); moreover, elimination is endergonic (+8.3 kcal/mol). In line with experiment, where **7b** was isolated, **E** is therefore predicted to be stable under experimental conditions with respect to F-elimination and Lewis acids need to be added to shift the equilibrium to the product side by removal of fluoride via salt metathesis, enforcing HDF of **2a**. The F-elimination **TS(E-H)** in the L_3Cu system is rather unusual and geometrically not late like the corresponding **TS(D-G)** in the L_2 system but rather central. On the one hand, the Cu-C bond is much more elongated (**D** 2.016, **E** 1.979, **TS(E-H)** 2.413, **TS(D-G)** 2.129 Å) and the forming C=C bond is shorter (**TS(E-H)** 1.384, **TS(D-G)** 1.407 Å). On the other hand, the forming Cu-F bond is much longer in the L_3 system (**TS(E-H)** 2.390, **TS(D-G)** 2.093 Å). Substantial charge separation occurs in both TS, (see **Table 2),** with the natural population analysis (NPA) charge on the eliminating F exceeding 0.6 e^-; charge separation is somewhat more extensive in the L_3 **TS(E-H)** and leads to a slightly higher dipole moment (5.6 D in L_2 vs. 6.1 D in L_3).

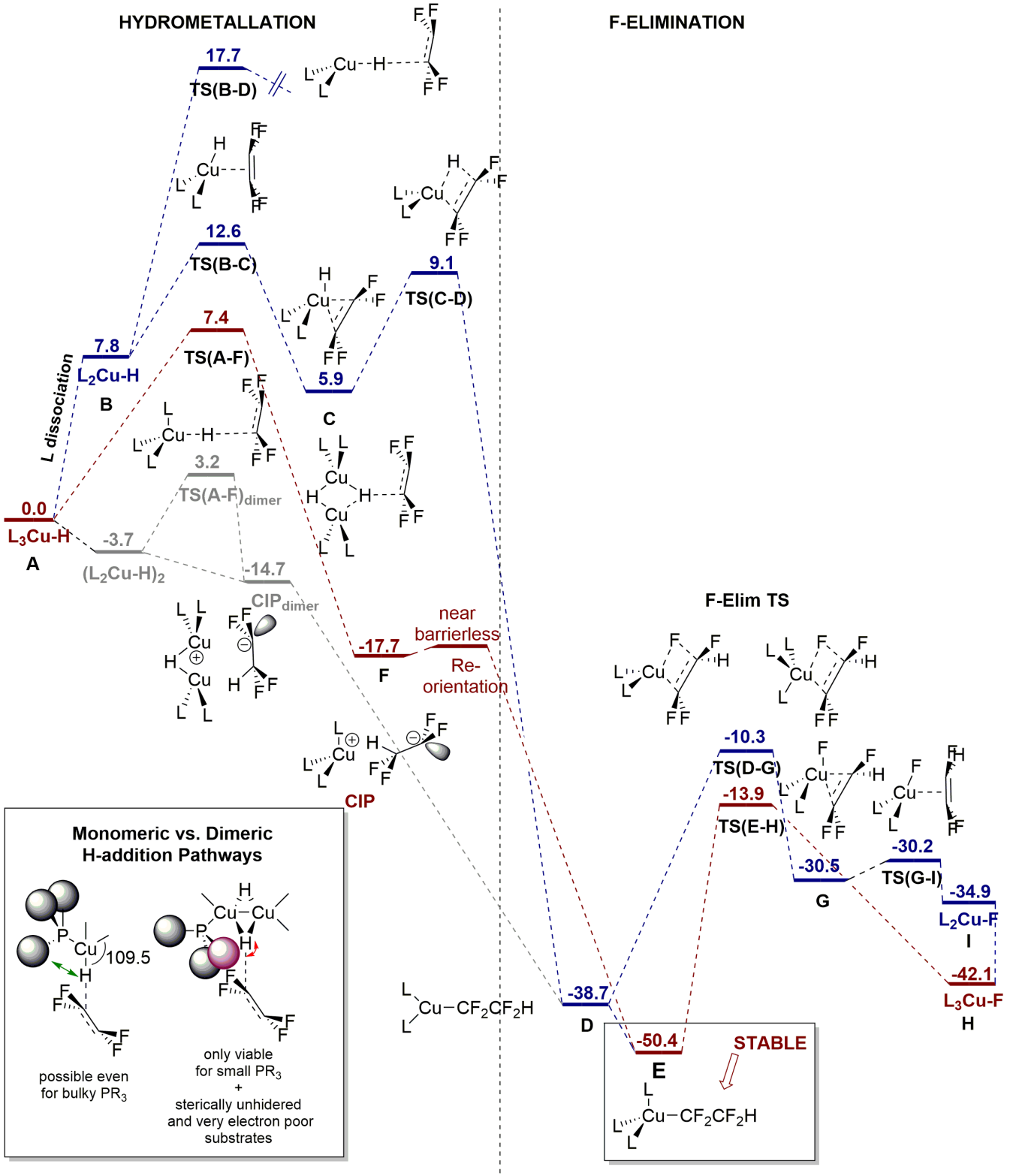

Figure 3. Potential energy surface (PES) for HDF of tetrafluoroethylene (**2a**) with L_3/L_2Cu-H. L = PMe_3. L_2 pathway in blue, L_3 pathway in maroon, dimeric $(L_2Cu\text{-}H)_2$ pathway in grey. CIP = contact ion pair. Level of theory TPSSh-D0(PCM)/TZ// TPSSTPSS(PCM)/DZ. T = 323 K. p = 0.1 bar. Solvent = benzene. Gibbs free energies in kcal/mol. PES after the high energy TS12-14 on the H-addition pathway in the L_2 system not shown. Only one symbolic phosphine ligand shown for monomeric vs. dimeric competition for clarity.

The extensive charge delocalization in the TS explains the experimentally observed rate dependence on the solvent. Wiberg bond indices (WBI)[33,34] support the notion that **TS(E-H)** is central in the L_3 system and less covalent, as WBIs for the Cu-F, Cu-C and F-C bonds are < 0.24, in all cases lower than in the corresponding L_2 system **TS(D-G)**. In contrast to

L_2, where elimination proceeds to RS **G** with copper-coordinated alkene, elimination in the L_3 system proceeds directly to L_3Cu-F (**H**) and the separated olefin **2b**. Decoordination of the olefin via **TS(G-I)** leads to L_2Cu-F **I**, which can be further stabilized via coordination of a third phosphine to form **H**. Overall, F-elimination in both the L_2 and L_3 system is reminiscent of the H-addition pathway in the L_3 system, which similarly shows extensive charge separation.

Table 2. NPA charges (q) on fragments and Wiberg bond indices (WBI) in L_2 **TS(D-G)** and L_3 **TS(E-H)** Elimination TS.

	q (e$^-$)		WBI		
Fragment	L_2	L_3	Bond	L_2	L_3
Cu	-0.02	-0.24	Cu-F	0.28	0.15
F_2C=CFH	-0.02	-0.05	Cu-C	0.34	0.24
F	-0.62	-0.67	F-C	0.37	0.23
			C=C	1.38	1.5

The first coordination sphere of copper in the F-elimination **TS(E-H)** can essentially be described as five-coordinate in the L_3 system, consisting of three phosphines, a FA and a fluoride ligand. However, Cu d^{10} does not possess the ability to engage in sp^3d-hybridization required for trigonal-bipyramidal binding of five ligands. The geometry of the P_3Cu fragment barely changes from the resting state **E**; P-Cu-P angles are 113(3)°for RS and TS, WBIs for the Cu-P bonds in **TS(E-H)** are with 0.72(1) even higher than in the L_2 system **TS(D-G)** with 0.64(1). Therefore, it appears that the system is better described as tetrahedral, with one coordination site being simultaneously occupied by both a fluoride and the alkene in the F-elimination TS (**Figure 4**). Both the HOMO and the HOMO-1 are concentrated on the Cu, F and the alkene, which supports this notion. The H-addition TS in the L_2 system is substantially higher in energy, as it only benefits from stabilization of the partial cationic charge by two phosphines, not three as in the L_3 system.

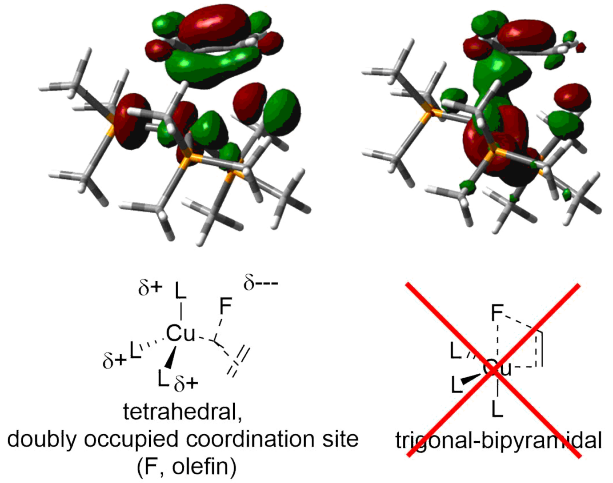

Figure 4. Top: HOMO (left) and HOMO-1 (right) of the L_3 F-elimination **TS(E-H). Bottom:** tetrahedral vs. trigonal-bipyramidal geometry in the L_3Cu(F, alkene) F-elimination TS. L = PMe_3.

In conclusion, in the PMe_3/Cu system, HDF proceeds preferentially via a three-step nucleophilic H-addition/Cu-C bond formation/F-elimination sequence either in an L_3 ligand environment along all steps or initially via a bimetallic L_2 environment. These pathways offer the possibility for lower barriers compared to the traditional monomeric L_2 insertion mechanism. Interestingly, the mechanism described here for FAs differs distinctively from the concerted SBM described by the group of Zhang for fluorinated arenes using a similar phosphine-stabilized copper hydride system.[25] We could not locate such TS for alkene systems. This presents a distinct difference from early transition metal systems, as in the case of Ti-catalyzed HDF, SBM TS could be found for both alkene and arene HDF systems,[7e,8a] although they are only kinetically relevant in the latter case.

Hydrometallation Pathway Competition. Substrate and Phosphine Influence. The model system indicates that there are (at least) three possible mechanistic pathways with low barriers for hydrometallation in present phosphine copper hydride systems and that the choice of phosphine ligand and FA substrate determines which of these pathways will be preferred.

Figure 5 shows trends in HM and F-Elimination barriers for FAs **2a**, **2b** and **2e** and L = PMe_3 (Table S8-S10) shows all relevant RS and TS). Barriers for hydrometallation via H-addition/Cu-C bond formation (L_3 pathway or dimeric pathway) or insertion (L_2 pathway) increase with decreasing fluorine content of the FA; i.e. no 'runaway' defluorination can occur. Due to the stabilization of the corresponding anions, hydrometallation in the bimetallic copper environment via H-addition/Cu-C carbon bond formation is the preferred mechanism for the highly fluorinated FAs **2a** and **2b**, and likely others like **1a**; hydrometallation via phosphine decoordination/insertion is preferred for more electron-rich FAs with lower fluorine content like **2e**. The preference for H-addition via the dimeric over the L_3 pathway diminishes with decreasing fluorine content.

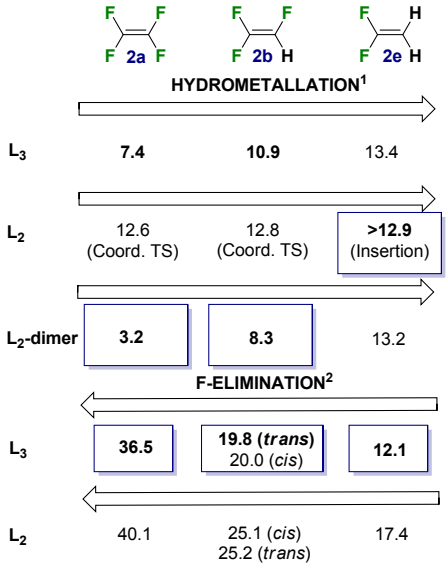

Figure 5. Trends in hydrometallation and F-elimination barrier heights for **2a**, **2b** and **2e** in the L_2 and L_3 ligand environment. L = PMe_3. [1] from the isolated reactants L_3CuH and FA. [2] from the L_3CuR resting state. Level of theory TPSSh-D0(PCM)/TZ//

TPSSTPSS(PCM)/DZ. T = 323 K. p = 0.1 bar. Solvent = benzene. Gibbs free energies in kcal/mol.

DFT predicts that the copper hydride dimer is only favored slightly (-0.3 kcal/mol) if L = $PMePh_2$ and that the L_3 pathway is preferred for $PMePh_2$/**2a** by 2 kcal/mol over the bimetallic mechanism and 8.4 kcal/mol over the phosphine decoordination/hydrometallation L_2 pathway. If L = PPh_3, then the H-addition L_3 pathway for **2a** is favored by 13.4 kcal/mol over the L_2 insertion pathway. Phosphine ligands that allow for an L_3 environment can subsequently enable HDF in systems where ligands enforcing a traditional L_2 mechanism fail.

F-elimination Pathway Competition. Substrate and Phosphine Influence. F-elimination becomes easier the lower the fluorine content of the forming FA is and is exergonic for both, **2b** and **2e** (Figure 5). The L_3 elimination mechanism is preferred for all three FAs by 4-5 kcal/mol. In the case of L = PPh_3, we were able to locate the L_3-F elimination TS for **2a** (-1.8 kcal/mol *vs.* L_2), however, all optimization attempts for **2b** lead to decoordination of one phosphine (see Supporting Information for an example structure for one TS with decoordinated phosphine). It appears that only phosphines with a small cone angle (Tolman cone angles:[35] PMe_3 118°, $PMePh_2$ 122°, PMe_2Ph 136°, PPh_3 145°) can allow for this TS also in cases where the alkyl fragment is less stabilized. Unlike the 'dagger-like' L_3 H-addition TS, the F-elimination TS needs significant space around the central metal to accommodate both the FA product and the fluoride ligand.

Ligand induced HDF selectivity differences. One of the striking observations in the present systems is the ability to tune the *cis/trans* product selectivity in the HDF of **2b** via the choice of the ancillary phosphine ligand. Stryker has noted similar observations in phosphine-stabilized copper(I) hydride mediated carbonyl hydrogenation, pointing out that the '*structure, reactivity and selectivity of copper(I) hydride catalysts are a complex and subtle function of the ancillary ligand*' and that those catalysts show an '*exceptional sensitivity … to structural variation in the ancillary ligand*'.[20]

We computationally tested the catalyst selectivity for several phosphines (**Table 3**), i.e. for the monodentate phosphines PPh_3, $PMePh_2$ and PMe_2Ph, and two bidentate phosphines with varying bite angle, dppe and Xantphos.

The experimentally observed selectivity for Xantphos (**2c**/**2d,** *cis/trans* 7:1 = $\Delta\Delta G^{\ddagger}_{50°C}$ = 1.4 kcal/mol) is nicely reproduced by DFT (1.2 kcal/mol), but the error for dppe is somewhat larger (predicted *cis* preference 0.4 kcal/mol, experimentally observed $\Delta\Delta G^{\ddagger}_{50°C}$ =1.4 kcal/mol, see SI). For $PMePh_2$ and PMe_2Ph, both, the L_2 pathway and the L_3 pathway are possible. DFT predicts that the L_3 pathway is preferred by 6-9 kcal/mol. Moreover, while F-elimination in the L_2 system is predicted to yield a 1:1 ratio of *cis* and *trans*, only the L_3 system is in line with the experimentally observed preference for *trans* elimination. The experimental selectivity for $PMePh_2$ and PMe_2Ph (*cis*/*trans* 1:4 = $\Delta\Delta G^{\ddagger}_{50°C}$ = 0.9 kcal/mol) appears to be somewhat overestimated (DFT: 1.5-2.0 kcal/mol). However, repeated product re-insertion into the Cu-F bond could diminish the kinetic *trans* preference of these catalysts somewhat, if regeneration of the catalyst is not fast enough. The possibility for re-insertion of FAs in the Cu-F bond could be successfully demonstrated by the experimental observation of **7b'**.

Table 3. Barriers for FHC=CFH elimination in various L_xCu-$CFHCF_2H$ systems. Level of theory TPSSh-D0(PCM)/TZ// TPSSTPSS(PCM)/DZ. Solvent = benzene. T = 323K, p = 0.1 bar. Energies in kcal/mol.

	cis $\Delta^{\ddagger}G_{elim}$	*trans* $\Delta^{\ddagger}G_{elim}$	ΔG_{Elim} (cis/trans)
L_2 systems			
dppe*	28.3	28.7	-9.6/-8.9
Xantphos*	25.6	26.8	-9.2/-8.9
PPh_3	23.8	26.1	-14.4/-13.8
$PMePh_2$	26.8	26.8	-8.9/-8.3
PMe_2Ph	28.1	27.9	-3.1/-2.5
L_3 systems			
$PMePh_2$	22.8	20.8	-8.9/-8.3
PMe_2Ph	20.4	19.0	-3.1/-2.5

* Resting state is assumed to be $L(PPh_3)Cu$-$CFHCF_2H$, L = dppe or Xantphos.[36]

Experimental trends, i.e. the preference for the *cis* isomer **2c** for ligands where F-elimination must proceed in the L_2 environment and for *trans* isomer **2d** for systems where it can proceed in the L_3 environment are very well reproduced. The model also correctly predicts that the F-elimination barrier is smaller in bidentate systems with larger bite angle (Xantphos vs. dppe). Product **2c** (*cis*) is preferred by 0.9 kcal/mol over **2d** (*trans*),[37] but clearly the ligand environment can modulate the product distribution in the present copper hydride systems, from enhanced *cis* preference all the way to a switch to *trans* preference.

We considered that the pronounced shift in selectivity could stem from short H-F contacts in the TS, as the *trans* TS often has more short contacts of this type. This has been postulated to lead to stabilizing TS interactions in other systems,[38,39] but NBO[40,41] does not locate any significant interactions between H-F in these systems (WBI < 0.002). Steric interactions could conceivably be responsible for the differences in the L_2 systems and, in line with experimental observations, a *cis* preference would be expected in this case. The distribution of steric bulk in L_2 systems as indicated by the topographic steric maps shown in Figure 6 leads to shorter ligand-FA contacts and thus increased steric repulsion in the *trans* TS (**Table 4**).

In the more *trans* selective system L_3, pseudo C_3-symmetric distribution of the phosphines equally distributes the steric bulk, offering no possibility for either of the two FHC=CFH isomers to avoid it (**Figure 6**). Unfavorable dipole-dipole interactions between the FA and L_xCuF can only play a role in the *cis* TSs (**Figure 7**) leading to **2c**; this is due to the relative orientation of the two dipoles in the *cis* TSs and the lack of a dipole for **2d**. Interestingly, the *trans* preference in the phosphine systems follows qualitatively Tolman's electronic parameter (Table 4), which point to electronic effects being responsible for the switch.

Although the unusual *cis* preference for the two isomers of FHC=CFH has been the subject of considerable research efforts in the past, it appears that no definitive conclusion on its origin has been reached, yet.[39-46]

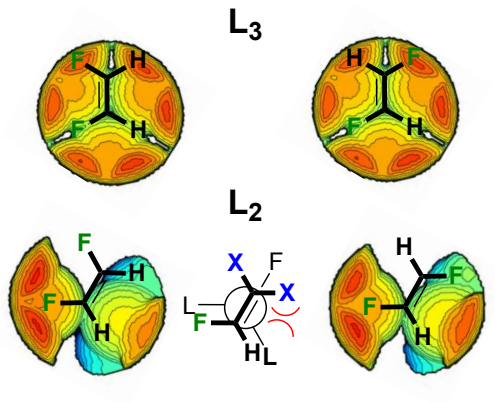

Figure 6. Symmetric distribution of steric bulk in L_3 systems and origin of *cis*-preference in L_2 systems (L = PMe_3) and map of steric bulk generated with SambVca 2.0 (webtool for analyzing catalytic pockets)[42] from L_3Cu-H; sphere radius of 3.5 Å.

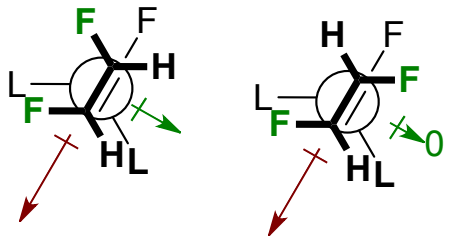

Figure 7. Unfavorable dipole-dipole interactions in L_3 TS leading to **2c** (left) vs lack of dipole-dipole interactions in L_3 TS leading to **2d** (right). L_2Cu-F fragment dipole orientation in maroon, FA dipole orientation in green.

Table 4. Ligand dependence of the preference for the *cis* FHC=CFH isomer in different L_2 and L_3 systems, Tolman's electronic parameter ν and differences between the shortest ligand-FA contacts ($l_{cis\text{-}trans}$) in the L_2 ligand environment and deformation energy difference of the FA fragments in the TS ($E_{Def.\ cis\text{-}trans}$).

	ΔΔG‡		ν	$L_{cis\text{-}trans}$	$E_{Def.\ cis\text{-}trans}$
	L_2	L_3			
Ph_3P	-2.5		2068.9	0.137	-2.2
Xantphos	-1.2			0.066	-0.4
dppe	-0.8			0.015	-1.2
Ph_2MeP	-0.2	2.0	2065.1	-0.023	-0.9/-1.0
$PhMe_2P$	0.0	1.5	2065.3	-0.025	-0.7/-0.3
Me_3P	0.1	0.4	2064.1	-0.048	-0.6/-1.9

Nonetheless, most authors appear to agree that the preference is of electronic origin.[40,47] In the absence of a definitive consensus on the origin of the *cis* preference, we deem a quantitative analysis of the trends here impossible. However, tentatively the preference switch can be explained as follows: The Hammond postulate assumes that electronic and steric changes from the reactants to the TS and further to the products occur gradually.[48,49] While TS of the L_3 type are central with respect to the overall TS geometry, they are later than L_2 type TS with respect to the forming olefin, as the forming C=C bond is much shorter (see also **Figure 2**). A shift from the L_2 to the L_3 environment should therefore increase the preference for the thermodynamic product; this is not observed for **2c**/**2d**. **Table 4** shows that the energy difference between the FA fragments in the *cis*/*trans* TS favors the *trans* isomer in all cases, indicating that the electronic stabilization of *cis*-1,2-difluoroethene occurs very late and that initially only the steric repulsion by the F atoms prevails. It appears that within the L_2 pathway, FA deformation and unfavorable dipole-dipole interactions in the *cis* TS favor the *trans* isomer, but this is more than compensated for by unfavorable steric interactions in the *trans* TS. L_2 leads preferentially to formation of the *cis* isomer **2c**. An increase in the FA-Cu distance in the L_3 environment weakens unfavorable dipole-dipole interactions in the *cis* TS and the symmetric distribution of steric bulk lessens steric differences. Subsequently, the FA deformation dominates, which leads to a preference for the *trans* isomer **2d**.

To the contrary, increased selectivity for the thermodynamic product upon L_2/L_3 switch is indeed observed experimentally in the HDF of the bulky α-trifluoromethyl styrene (**8a**). Use of the small cone angle phosphite $P(OEt)_3$ increases the selectivity for the thermodynamic product *Z*-β-fluoro-α-methyl styrene (**8c**) from 2.8:1 (Xantphos/$PMePh_2$) to 7.2:1 [$P(OEt)_3$] (DFT, L = $P(OMe)_3$: $\Delta\Delta G^{\ddagger}$ L_2 1.3 kcal/mol, L_3 2.3 kcal/mol). No HDF is observed for **2b** with this ligand class. Phosphites are electron-poor and DFT indicates that F-elimination in such a system could lead to F/OR exchange on the organophosphite ligand during HDF of **2a**.[53]

Experimental Mechanistic Studies. To confirm these DFT revelations, mechanistic studies were carried out. As the L_2CuH systems like Xantphos presumably follow the previously reported insertion-elimination mechanism, as supported by DFT calculations (*vide supra*), mechanistic studies were focused on the L_3CuH HDF mechanism using $PMePh_2$.

Control experiments for the HDF of trifluoroethylene, **(2b),** confirmed that all three components of the reaction mixture are required. The product ratio of the HDF of **2b** using $PMePh_2$ is altered (**2c**:**2d**, 1:1) when no silane is present; no such alteration is observed for Xanthphos. This experiment suggests that re-insertion of **2c**/**2d** into Cu-F occurs if no silane is present as noted above for TFE (**2a**). Similarly, TMDS does not effect HDF at RT without a source of copper. Nor does the mixture of phosphine and TMDS, confirming that the copper plays a crucial role in this HDF reaction. However, when the reaction was attempted with varying concentrations of silane; no rate dependence was observed. As a significant rate increase with increasing solvent polarity was observed, the silane substituents were varied to elaborate further on its role. Interestingly, the reaction only progresses smoothly at RT when either triphenylsilane (Ph_3SiH) or TMDS are used. With triethoxysilane [$(EtO)_3SiH$] the reaction turns over once at RT and then ceases operation. If heated to 45 °C, the reaction progresses with some loss of selectivity. This is reminiscent of Lentz's observations in Ti(III) complex-catalyzed HDF, where $(EtO)_3SiH$ led to fast catalyst deactivation via formation of alkoxytitanium compounds.[29] The alkyl silanes either require heating (i.e. triethylsilane) or are ineffective (i.e. triisopropylsilane). Interestingly, diphenylsilane also does not work at room temperature, and requires heating to 70 °C but the reaction mixture quickly becomes black. The most productive silanes are thus those with somewhat more electron-withdrawing functional groups.

Based on the stoichiometric reactions of $PMePh_2$/$(PPh_3CuH)_6$/**2b**, a fast equilibrium between the resulting products is suspected. In line with observations (see above), this would lead to an increased **2c**/**2d** ratio tending towards the thermodynamic distribution. On this note, as the rate of Cu-F to Cu-H conversion becomes slow, a secondary reaction becomes competitive, leading eventually to complete catalyst deactivation via formation of a copper(I)-alkenyl complex by formal HF elimination (**Scheme 9**). Additionally, formation of 1,1,1,2-tetrafluoroethane (**2b'**) suggests that the generated Cu-alkyl reacts quickly with HF, explaining why it is not observed over the reaction course.

To probe the elementary steps further, the source of hydride was confirmed using the Si-D reagent. When the reaction was carried out with stoichiometric amounts of Cu-H and a slight excess of triethylsilyl deuteride, the major product contained mostly protons, confirming that Cu-H adds to the FA, and that the silane's role is likely restricted to Cu-H regeneration.

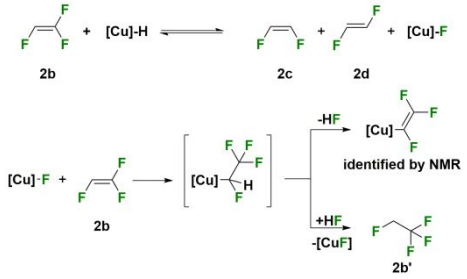

Scheme 9. Reaction of copper hydride with **2b** leading to formation of a copper trifluorovinyl complex and R-134a (**2b'**).

Effects controlling selectivity for the L_2CuH or L_3CuH mechanism. With the DFT and experimental support for the L_3CuH mechanism, other FAs were examined to determine the effects of FA substitution on the ability to access the L_3CuH mechanism. For consistency with reactions using the Xantphos catalyst, these reactions were carried out in benzene at 45 °C. First, mono-substituted FAs were explored to determine if β-fluoride elimination is crucial in accessing analogs of **TS(E-H)**. As such, FAs $XFC{=}CF_2$ [X = Cl (**3a**), I (**3b**) or OCF_3 (**4a**)] were used. Unfortunately, when iodotrifluoroethylene, **3b**, was treated with stoichiometric copper hydride, $HFC{=}CF_2$, **2b**, was observed as the major product, independent of the choice of ligand. It is suspected that this occurs via *σ*-bond metathesis of the C-I bond. However, with chlorotrifluoroethylene (**3a**), when using Xantphos, the observed product was a mixture of *cis-/trans*-1,2,-difluoroethylene, **2c/2d**. This result suggests that the first HDF step produces 1-chloro-1,2-difluoroethylene (**3a'**) arising from addition of the hydride to the CF_2 carbon. This new alkene is considerably more reactive than **3a**, such that addition of Cu-H to **3a'** dominates. Consistent with this result, $PMePh_2$ yields the same product distribution as that observed with Xantphos, indicating that β-fluoride elimination is necessary to access analogues of **TS(E-H)**. To confirm this, the HDF of **4a** was attempted with $PMePh_2$ and $P(OEt)_3$ and **2c,d** were produced in the same ratio as the Xantphos reaction (*vide supra*). β-X elimination (X = Cl or OCF_3), excluding fluoride, generally proceeds through the known analogous transition states of **TS(D-G)**.

On another note, the low activation energy for the L_3CuH hydride addition mechanism could explain why $P(OEt)_3$ is competitive in efficiency in the HDF of **1a** with the dppf or Xantphos ligands. It would be expected, however, that accessing analogues of **TS(A-F)**, depends on a delicate balance of the stabilization of Cu^+ and the carbanion (Alk). To explore this idea, 1,1-difluoroethylene (**2e**) was used, as the Xantphos catalyst cannot hydrodefluorinate this substrate (**Scheme 10, bottom**). Interestingly, use of $P(OEt_3)$ also afforded no HDF product from **2e**. In contrast, the $PMePh_2$ Cu-H catalyst led to efficient HDF of **2e** to a 3:1 mixture of vinyl fluoride (**2f**) and ethylene (**Scheme 10, Top**) although calculations show that this substrate could be hydrometallated via both mechanisms (**Figure 5**). As such, a larger cone-angle, stronger σ-donating phosphine ligand, PCp_3, was also tested with no HDF product detected. Again, because ligand size is so important, $PMePh_2$ likely leads to greater Cu^+ stabilization, thus balancing the destabilized carbanion, H_2CR^-, in the L_3CuH mechanism.

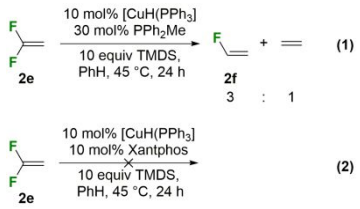

Scheme 10. Hydrodefluorination of 1,1-difluoroethylene (**2e**)

These results suggest that an electronic limit to the HDF of FAs via the L_3CuH mechanism exists (i.e., in cases where the stabilization of the Cu^+ is not great enough to offset Alk^- destabilization). Therefore, alkyl-substituted FAs were tested next (**Scheme 11**).

In this case, 1,1,1-trifluoropropene (**9**) was subjected to HDF to generate **1f** in situ (**Eq. 11.1**). As expected, no further HDF was observed using the Xantphos or $PMePh_2$ system. On addition of a stabilizing element to Alk^-, HDF through the L_3CuH mechanism should proceed. When α-trifluoromethyl styrene (**8a**) was used to generate β-difluoro-α-methyl styrene (**8b**) in situ, Xantphos and $PMePh_2$ yielded the same product distribution of *E*/*Z*- β-fluoro-α-methyl styrene (**8c,d**) in a ratio of 2.8:1 (**Eq. 11.2**). The steric congestion arising from addition, with the =CPhMe carbon bonded to copper, now proves too much to accommodate the third $PMePh_2$ ligand required for the L_3 mechanism. As such, the L_2 mechanism dominates

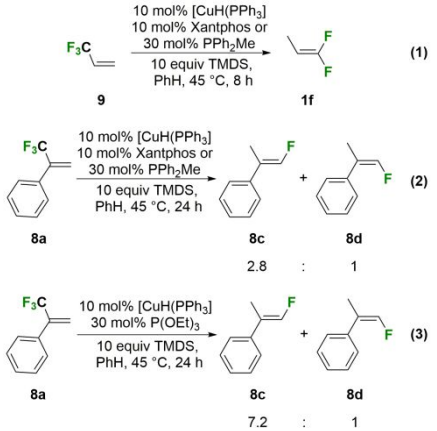

Scheme 11. Hydrodefluorination of allyl trifluoropropene (top) and α-trifluoromethyl styrene (bottom)

for control of the product ratio in both cases. Nevertheless, if our hypothesis is correct, even the weaker σ-donating but smaller ligand should function, due to the Alk- benzylic stabilization. Indeed when $P(OEt)_3$ was used, the HDF of **8a** to **8b** and on to **8c,d** proceeded smoothly to provide an increased product ratio of 7.2:1 (**Eq. 11.3**). Apparently, the L_3 mechanism reinforces the E/Z ratio as **8c** is both the least polar and most thermodynamically stable, as confirmed by DFT (*vide supra*).

CONCLUSION

In summary, new P-ligated copper hydride complex-catalyzed routes for the HDF of fluoroalkenes using silanes have been developed. With our technology, hexafluoropropene (**1a)** can be selectively converted to fourth-generation refrigerant CH_2=$CF(CF_3)$ (**1d**) or to 1,1-difluoropropene (**1f**). While the (dppe)Cu-H system stops at the double HDF, giving the highest yield of **1d**, small cone-angle, less electron-rich $P(OEt)_3$ allows for the quadruple HDF of **1a** to **1f**. On evaluating the HDF substrate scope we found that use of a smaller cone-angle, electron-rich ligand such as $PMePh_2$ leads to L_3Cu-H reactivity with electron-poor or bulky fluoroalkenes not observed with the L_2CuH systems. DFT studies revealed an exceptional, ligand- and substrate-dependent mechanistic flexibility in these copper(I) hydride systems ranging from monomeric insertion/elimination to bimetallic or monomeric hydride transfer mechanisms. In the latter, F-elimination involves a doubly-occupied coordination site at copper. Both hydrometallation and F-elimination in the L_2 as well as the L_3 system proceed via TSs showing significant charge separation, explaining the experimentally observed rate dependence on the solvent. DFT results are nicely in line with experimental observations. We propose that the phosphine choice can modulate the position of the F-elimination TS with respect to the product and thereby modulate product selectivity, as experimentally observed for **2b** and **8a**. It appears that in the case of **8a**, tuning the position of the F-elimination TS reinforces the preference for the thermodynamic product. In the case of **2b**, the switch from L_2 to L_3 environment leads to a switch from thermodynamic to kinetic product. We believe that this effect can be traced to a breakdown of the assumption that steric and electronic changes occur gradually from RS to TS to product in this specific case.

With tetrafluoroethylene both (P-P)CuH and P_3CuH complexes (**7a,b**) could be successfully isolated and are currently being assessed for the introduction of the 1,1,2,2-tetrafluoroethyl ($-CF_2CF_2H$) moiety to organic electrophiles.[54]

EXPERIMENTAL SECTION

General Procedures. Experiments were conducted under nitrogen, using Schlenk techniques or an MBraun glove box. All solvents were deoxygenated by purging with nitrogen. Tetrahydrofuran (THF) and toluene were dried on columns of activated alumina using a J. C. Meyer (formerly Glass Contour®) solvent purification system. Chlorobenzene, *m*-dimethoxybenzene, benzene, cyclopentyl methyl ether (CPME) and benzene-d_6 (C_6D_6) were dried by stirring over activated alumina (ca. 10 wt. %) overnight, followed by filtration. All solvents were stored over activated (heated at ca. 250 °C for >10 h under vacuum) 4 Å molecular sieves. Glassware was oven-dried at 120 °C for >2 h. The following chemicals were obtained commercially, as indicated: Dimethylformamide (DMF, Alfa Aesar Anhydrous 99.8%), hexafluoropropene (**1a**, Synquest 98.5%), trifluoroethylene (**2b**, Synquest 98%), chloro trifluoroethylene (**3a**, Synquest, 99%), iodo trifluoroethylene (**3b**, Synquest, 97%), trifluoromethyl trifluorovinyl ether (**4a**, Synquest, 99%), vinylidene difluoride (**2e**, Arkema Inc., 99%), alpha-trifluoromethyl styrene (**8a**, Synquest, 97 %), hexafluorocyclobutene (**5a**, Synquest 98%), 3,3,3-trifluoropropene (**9**, Synquest, 99%), perfluoro(4-methyl-2-pentene) (**6b**, Synquest, 95%), perfluoro(2-methyl-2-pentene) (**6a**, Synquest, 96%), triethylesilane (Sigma-Aldrich, 99%), triethyl(silane-*d*) (Sigma-Aldrich, 97 atom % D), triisopropylsilane (Oakwood chemicals, 98%), triphenylsilane (Oakwood chemicals, 97%), triethoxysilane (Sigma-Aldrich, 95%), diphenylsilane (Oakwood chemicals, 97%), tetramethyldisiloxane (TMDS, Sigma-Aldrich, 97 %), poly(methyl-hydrosiloxane) (PMHS, Sigma-Aldrich, average M_n: 1,700-3,200), triphenylphosphine (PPh_3, Oakwood chemicals, 99%), tri(*o*-tolyl)phosphine ($P(o\text{-tolyl})_3$, Alfa Aesar, 98%), 2-di-tert-butylphosphino-2′,4′,6′-triisopropylbiphenyl (tbuXphos, Sigma-Aldrich, 97%), 1,2-bis(diphenylphosphino) ethane (dppe, Strem chemicals, 99%), 1,1'-bis(diphenylphosphino) ferrocene (dppf, Accela ChemBio Inc., 99%), 4,5-bis(diphenylphosphino)-9,9-dimethylxanthene (Xantphos, Accela ChemBio Inc., 99%), triethylphosphite ($P(OEt)_3$, Sigma-Aldrich, 98%), triphenylphosphite ($P(OPh)_3$, Alfa Aesar, 97%), tri-ortho-tolyl phosphite ($P(O\text{-}o\text{-tolyl})_3$, Alfa Aesar), methyldiphenylphosphine ($PMePh_2$, Acros Organics, 99%), dimethylphenylphosphine (PMe_2Ph, Acros Organics, 97%). The following chemicals were synthesized as previously reported: 1,3-bis(2,6-diisopropylphenyl)imidazolidin-2-ylidene (SIPr)[55] and $[(PPh_3)CuH]_6$.[56] Tetrafluoroethylene (**2a**) was prepared by pyrolysis of polytetrafluoroethylene (Scientific Polymer Products, powdered) under vacuum, using a slightly modified literature procedure [10-20 mTorr, 650 °C, 30 g scale, product stabilized with R(+)-limonene (Aldrich, 97%), giving **2a** of ca. 97% purity][57] or by pyrolysis of $KO_2CCF_2CF_3$ under vacuum, producing TFE Safe Supply®.[58] ^{1}H, ^{19}F, ^{31}P{^{1}H}, and ^{13}C{^{1}H} NMR spectra were recorded on a 300 MHz Bruker Avance instrument at room-temperature (21-23 °C) unless stated otherwise. ^{1}H NMR spectra were referenced to residual proton peaks associated with the deuterated solvents (C_6D_6: 7.16 ppm). ^{19}F NMR spectra were referenced to internal standard α,α,α-trifluorotoluene (CF_3Ph) [unless stated otherwise] (Sigma-Aldrich, 99%, deoxygenated by purging with nitrogen, stored over activated 4 Å molecular sieves), set to – 63.5 ppm. ^{31}P{^{1}H} NMR data were referenced to external H_3PO_4 (85 % aqueous solution), set to 0.0 pm. Electrospray ionization mass spectral data were collected using an Applied Biosystem API2000 triple quadrupole mass spectrometer. Elemental analyses were performed by Ján Veizer Stable Isotope Laboratory, University of Ottawa (Ottawa, Ontario, Canada). Note that the NMR spectra (^{1}H, ^{19}F, ^{19}F{^{1}H}, and ^{31}P{^{1}H} for the title compounds are displayed at the end of the Supporting Information (Figures S4-44).

General Experimental Procedure for Hydrodefluorination of Gaseous Fluoroalkenes, NMR Scale. $[(PPh_3)CuH]_6$ (5 mg, 0.02 mmol, 10 mol %) was placed in a 7″ nmr tube and mixed with 400 μL of solvent. A ligand (31 mol % or 11 mol %) and silane (10 equiv) were added. The tube was capped with a rubber septum, removed from the glovebox, further sealed by tightly wrapping the cap with a

strip of parafilm and shaken to ensure a homogeneous solution. 3 mL of gaseous fluoroalkene were then added to the reaction via air-tight syringe. The reaction was monitored by ^{19}F NMR over 8 hours at various temperatures. See Figure S4-34 for ^{1}H NMR and ^{19}F NMR spectra and Table S1 for ^{19}F NMR data. Compounds **1b**[59], **1c**[59], **1d**[60], **1e**[61], **1f**[4], **2c**[62], **2d**[62], **2f**[62], **4b**[63], **5b**[64] and **5c**[64], **5d**[64] were identified using available literature data.

*Z-3,3,3,2,1-pentafluoropropene (**1b**)*. ^{1}H NMR (300 MHz, C_6D_6): δ 6.13 (ddq, $^{2}J_{HF}$ = 68, $^{3}J_{HF}$ = 15, $^{4}J_{HF}$ = 1 Hz, =CHF). ^{19}F NMR (282 MHz, C_6D_6): -72.59 (ddq, $^{3}J_{FF}$ = 14, $^{4}J_{FF}$ = 6, $^{4}J_{FH}$ = 1 Hz, CF_3), -155.07 (ddq, $^{2}J_{FH}$ = 68, $^{3}J_{FF}$ = 7, $^{4}J_{FF}$ = 6 Hz, =CFH), -158.97 ppm (ddq, $^{3}J_{FH}$ = 15, $^{3}J_{FF}$ = 7, $^{4}J_{FF}$ = 6 Hz, =CF(CF_3)).

*E-3,3,3,2,1-pentafluoropropene (**1c**)*: ^{1}H NMR (300 MHz, C_6D_6): δ 5.93 (dd, $^{2}J_{HF}$ = 68, $^{3}J_{HF}$ = 4 Hz, = CHF). ^{19}F NMR (282 MHz, C_6D_6): -70.09 (dd, $^{3}J_{FF}$ = 19, $^{4}J_{FF}$ = 12 Hz, CF_3), -165.93 (ddq, $^{2}J_{FH}$ = 68, $^{3}J_{FF}$ = 137, $^{4}J_{FF}$ = 19 Hz, =CFH), -180.12 ppm (ddq, $^{2}J_{FH}$ = 4 $^{3}J_{FF}$ = 137, $^{4}J_{FF}$ = 12 Hz, =CF(CF_3)).

*3,3,3,2-tetrafluoropropene (**1d**)*: ^{1}H NMR (300 MHz, C_6D_6): δ 4.36 (ddq, $^{2}J_{HH}$ = 5, $^{3}J_{HF}$ = 13, $^{3}J_{HF}$ = 1 Hz, =CH_{2cis}), 4.49 (br dd, $^{2}J_{HH}$ = 4, $^{3}J_{HF}$ = 52 Hz, =CH_{2trans}). ^{19}F NMR (282 MHz, C_6D_6): -73.28 (d, $^{3}J_{FF}$ = 10 Hz, CF_3), -124.12 ppm (ddq, $^{3}J_{FH}$ = 52, $^{3}J_{FH}$ = 13 Hz, $^{3}J_{FF}$ = 10 Hz. =CF(CF_3)).

*1,1,2-trifluoropropene (**1e**)*: ^{19}F NMR (282 MHz, C_6D_6): -106.32 (ddq, $^{2}J_{FF}$ = 93, $^{3}J_{FF}$ = 32, $^{4}J_{FH}$ = 5 Hz, =CF_{2cis}), -126.15 (ddq, $^{2}J_{FF}$ = 93, $^{3}J_{FF}$ = 115, $^{4}J_{FH}$ = 5 Hz, =CF_{2trans}), -167.19 ppm (ddq, $^{3}J_{FF}$ = 115, $^{3}J_{FF}$ = 32, $^{3}J_{FH}$ = 17 Hz, =CF(CH_3)).

*1,1-difluoropropene (**1f**)*: ^{19}F NMR (282 MHz, C_6D_6): -89.67 (ddq, $^{2}J_{FF}$ = 50, $^{3}J_{FH}$ ≈ $^{4}J_{FH}$ = 3 Hz, =CF_{2trans}), -93.45 ppm (ddq, $^{2}J_{FF}$ = 50, $^{3}J_{FH}$ = 25, $^{4}J_{FH}$ = 2 Hz, =CF_{2cis}).

*Z-1,2-difluoroethylene **(2c)***:^{1}H NMR (300 MHz, C_6D_6): δ 5.54 (m). ^{19}F NMR (282 MHz, C_6D_6): δ -163.09 ppm (m).

*E-1,2-difluoroethylkene **(2d)***: ^{1}H NMR (300 MHz, C_6D_6): δ 6.68 (m). ^{19}F NMR (282 MHz, C_6D_6): -187.73 ppm (dd, $^{2}J_{FH}$ = 49, $^{3}J_{FH}$ = 30 Hz).

*Vinyl fluoride (**2f**)*: ^{1}H NMR (300 MHz, C_6D_6): δ 6.14 (ddd, $^{2}J_{HF}$ = 85, $^{3}J_{HH}$ = 13, $^{3}J_{HH}$ = 5 Hz), 4.54 (ddd, $^{3}J_{HF}$ = 20, $^{2}J_{HH}$ = 12, $^{3}J_{HH}$ = 3 Hz), 4.00 (ddd, $^{3}J_{HF}$ = 54, $^{2}J_{HH}$ = 5, $^{3}J_{HH}$ = 3 Hz). ^{19}F NMR (282 MHz, C_6D_6): -115.97 ppm (ddd, $^{2}J_{FH}$ = 85, $^{3}J_{FH}$ = 54, $^{3}J_{FH}$ = 20 Hz).

Z-Trifluoromethyl-1,2-difluorovinyl ether (***4b***): ^{19}F NMR (282 MHz, C_6D_6): -54.78 (m, OCF_3), -118.28 (m, F), -122.22 ppm (dm, $^{2}J_{FH}$ = 59 Hz).

*1,4,4-trifluorofluorocyclobutene (**5b**)*: ^{19}F NMR (282 MHz, C_6D_6): δ -106.52 (m, 2F), -113.45 ppm (m, 1F).

*1,2-difluorofluorocyclobutene (**5c**)*: ^{1}H NMR (300 MHz, C_6D_6): δ 1.67 (m, 2H) ppm. ^{19}F NMR: (282 MHz, C_6D_6) -118.57 ppm (m, 4F).

*1-fluorocyclobutene (**5d**)*: ^{19}F NMR (282 MHz, C_6D_6): -84.23 ppm (m, 1F).

General Experimental Procedure for Hydrodefluorination of Non-Gaseous Fluoroalkenes, NMR Scale.

$[(PPh_3)CuH]_6$ (5 mg, 0.02 mmol, 10 mol %) was placed in a 7″ nmr tube and mixed with 400 μL of solvent. A ligand (31 mol % or 11 mol %), silane (10 equiv, 1.45 mmol) and fluoroalkene (0.15 mmol) were added. The tube was capped, removed from the glovebox, further sealed by tightly wrapping the cap with a strip of parafilm and shaken to ensure a homogeneous solution. The reaction was monitored by ^{19}F NMR over 8 h at various temperatures. See Figure S35-38 for ^{19}F NMR spectra and Table S1 for ^{19}F NMR data. Compounds **6c**[65], **8b**,[66] **8c**[66] and **8d**[66] were identified using available literature data.

*1,1,4,4,5,5,5-heptafluoro-2-methylpent-1-ene (**6c**)*. ^{1}H NMR (300 MHz, C_6D_6): δ 2.13 (t, $^{3}J_{HF}$ = 19 Hz, CH_2), 1.22 (m, CH_3). ^{19}F NMR (282 MHz, C_6D_6): -86.42 (s, CF_3), -92.00 (d, $^{2}J_{FF}$ = 44 Hz, 1F), -92.64 (d, $^{2}J_{FF}$ = 44 Hz, 1F), -117.07 ppm (tm, $^{3}J_{FH}$ = 19 Hz, CF_2).

*1,1-difluoro-2-methyl-2-phenylethyl-1-ene (**8a**)*: ^{1}H NMR (300 MHz, C_6D_6): δ 1.59 (dd, $^{4}J_{HF}$ ≈ $^{4}J_{HF}$ = 3 Hz, Me). ^{19}F NMR (282 MHz, C_6D_6): -91.99 (dq, $^{2}J_{FF}$ = 44, $^{4}J_{FH}$ = 3 Hz), -92.30 ppm (dq, $^{2}J_{FF}$ = 44, $^{4}J_{FH}$ = 2 Hz).

*(E)-1-fluoro-2-methyl-2-phenylethyl-1-ene (**8b**)*: ^{1}H NMR (300 MHz, C_6D_6): δ 7.4 – 6.9 (Ar), 6.58 (dq, $^{2}J_{HF}$ = 85, $^{4}J_{HH}$ = 2 Hz, $1H_{(FHC=)}$), 1.80 (dd, $^{4}J_{HF}$ = 4, $^{4}J_{HF}$ = 2 Hz, Me). ^{19}F NMR (282 MHz, C_6D_6): -131.66 ppm (dq, $^{2}J_{FF}$ = 85, $^{4}J_{FH}$ = 4 Hz).

*(Z)-1-fluoro-2-methyl-2-phenylethyl-1-ene (**8c**)*: ^{1}H NMR (300 MHz, C_6D_6): δ 7.4 – 6.9 (Ar), 6.22 (dq, $^{2}J_{HF}$ = 84, $^{4}J_{HH}$ = 2 Hz, $1H_{(FHC=)}$), 1.80 (dd, $^{4}J_{HF}$ = 5, $^{4}J_{HF}$ = 2 Hz, Me). ^{19}F NMR (282 MHz, C_6D_6): -131.66 ppm (dq, $^{2}J_{FF}$ = 84, $^{4}J_{FH}$ = 5 Hz).

Synthesis of [($PMePh_2$)$_3$Cu(CF_2CF_2H)] (7a). The red complex $[(PPh_3)CuH]_6$ (3.16 g, 9.69 mmol based on monomeric unit), PPh_2Me (6.01 g, 30 mmol) and TMDS (1.4 mL, 8 mmol or 16 mmol hydride equivalents) were placed in a 350 mL ampule and mixed with 30 mL of benzene. The reaction vessel was attached via a three-way valve to a **2a**:CO_2 canister with a regulator and a Schlenk line. The solution was degassed using a regular freeze/pump/thaw method. The **2a**:CO_2 was added to the degassed solution with the regulator set to 5 psi and the reaction mixture stirred at 70 °C. After 10 minutes, the regulator pressure dropped to 0 and more **2a**:CO_2 was added. After ~2 h, the solution became clear with some black precipitate. The solvent was removed in vacuo, leaving a thick liquid. 10 mL of Et_2O was added, and the solution was then filtered through a Celite-padded fritted funnel (30 mL medium pore). The ampule was rinsed 2 more times with 10 mL of Et_2O. All volatiles were removed in vacuo and 50 mL of methylcyclohexane were added to the solution. Upon standing, the product crystallized from solution. The white microcrystalline powder was collected (30 mL medium-pore fritted funnel), triturated with pentane (2 x 20 mL), and dried in vacuo to yield 5.17 g of **7a** (6.8 mmol, 69 % based on $[(PPh_3)CuH]_6$). ^{1}H NMR (300 MHz, C_6D_6): δ 7.23 (m, 16H, $PMePh_2$), 6.89 (m, 25H, $PMePh_2$), 6.75 (tt, 1H, $^{2}J_{HF}$ = 52, $^{3}J_{HF}$ = 5 Hz, -CF_2H), 1.55 (br, 12H, $PMePh_2$) ppm. ^{19}F NMR (282 MHz, C_6D_6): −96.68 (dt, $^{3}J_{FF}$ = $^{3}J_{FH}$ = 5 Hz, CF_2), -124.89 ppm (dt, $^{2}J_{FH}$ = 52,$^{3}J_{FF}$ = 5 Hz, -CF_2H). ^{31}P{^{1}H} NMR (121 MHz, C_6D_6): −20.0 ppm (br, $PMePh_2$). Anal. Calcd for $C_{41}H_{40}CuF_4P_3$: C, 64.35, H, 5.27. Found: C, 60.49, H, 5.31. (These values reflect those expected for phosphine oxidation prior to combustion. Anal. Calc. for $C_{41}H_{40}CuF_4O_3P_3$: C, 60.56, H, 4.96.) See Figures S40−S42 for ^{1}H, ^{19}F, and ^{31}P{^{1}H} NMR spectra.

Synthesis of [(Xantphos)Cu(CF_2CF_2H)] (7b). The red complex $[(PPh_3)CuH]_6$ (25 mg, 0.08 mmol based on monomeric unit), Xantphos (40 mg, 0.08 mmol) and TMDS (2 μL, 0.01 mmol) were placed in a 7" NMR tube mixed with

400 μL of C_6D_6. The tube was capped with a rubber septum, removed from the glovebox, further sealed by tightly wrapping the cap with a strip of parafilm and shaken to ensure a homogeneous solution. 3 mL of gaseous **2a** was added to the reaction via air-tight syringe. The reaction was monitored by ^{19}F NMR over 8 hours at various temperatures. Compound **7b** was identified by comparing to **7a**. ^{19}F NMR (282 MHz, C_6D_6): −103.9 (br m, CF_2), -125.45 ppm (br dm, $^2J_{FH}$ = 52, -CF_2H). $^{31}P\{^1H\}$ NMR (121 MHz, C_6D_6): −16.74 ppm (br m, Xantphos). See Figures S44−S45 for ^{19}F and $^{31}P\{^1H\}$ NMR spectra.

Computational Details. All geometries were fully optimized using the Gaussian 09 software package[67] in combination with an external optimizer (PQS, OPTIMIZE routine of Baker[68,69]) and the BOpt software package.[70] Following the protocol proposed in ref.[71], all relevant minima and transition states were fully optimized at the TPSSTPSS level[72] of theory employing correlation-consistent polarized valence double-ζ Dunning (DZ) basis sets with cc-pVDZ quality[73,74] from the EMSL basis set exchange library, using a small core pseudo-potential on Cu.[75] The density fitting approximation (Resolution of Identity, RI) [76-79] was used at the optimization stage and for single-point energy corrections. Solvent effects (benzene, ε = 2.2706) were included with the polarizable continuum model approach (PCM) at both stages.[80] All calculations were performed at the standard Gaussian 09 SCF convergence using an ultrafine grid [Scf=Tight and Int(Grid=ultrafine)]. The nature of each stationary point was checked with an analytical second-derivative calculation (no imaginary frequency for minima, exactly one imaginary frequency for transition states, corresponding to the reaction coordinate). The accuracy of the TS was confirmed with an IRC scan on preliminary gas phase calculations. Transition states were located using a suitable guess and the Berny algorithm (Opt=TS)[81] or a relaxed potential energy scan to arrive at a suitable transition-state guess, followed by a quasi-Newton or eigenvector-following algorithm to complete the optimization.

Final single-point energies were calculated at the TPSSh level of theory[82] employing triple-ζ Dunning (TZ) basis sets (cc-pVTZ quality).[73] Grimme dispersion corrections without damping (keyword -zero) were added at this stage using the standalone dftd3 program.[83,84] Enthalpies and Gibbs free energies were then obtained from TZ single-point energies and thermal corrections from the TPSSTPSS(PCM)/cc-pVDZ-(PP) vibrational analyses; entropy corrections were scaled by a factor of 0.67 to account for decreased entropy in the condensed phase.[85-87] $\Delta\%V_{Bur}$ was calculated using the SambVca 2.0 program.[43] Maps of steric bulk were generated using the same program. NBO 3.1 was used for NBO analysis.[88]

The correct prediction of copper-phosphine bond strengths is crucial for the competition of mechanisms described in this paper. Metal-phosphine bond strengths are known to be challenging to predict and dispersion corrections are critically needed for their accurate description.[36] To our knowledge, no accurate experimental data is available for Cu-P bonds. In the absence of this data, we decided to benchmark the protocol against available gas phase bond dissociation energies of copper complexes with labile binding of ligands,[31] i.e. Cu(0)-NH_3,[90] Cu^+CO[91] and the 1st and 2nd binding energies in $Cu^+(ethene)_2$[92] and $Cu^+(acetonitrile)_4$[93]. A labile metal phosphine bond was included in the benchmark via the complex $Ni(CN)_2(PEt_3)_3$, in the solvents dichloroethane and ethanol.[36] For this set of 8 bonds, the protocol including Grimme's dispersion corrections with no damping produces an MAD of 1.8 kcal/mol. Becke-Johnson damping leads to an overestimation of bond dissociation energies and a higher discrepancy (MAD 4.2 kcal/mol). Finally, in a limited test set, we included dispersion corrections during optimization via the use of the B97D functional,[89] but this did not noticeably change the predictions.

ASSOCIATED CONTENT

Supporting Information. This material is available free of charge via the Internet at http://pubs.acs.org.

Addition crystallographic information, DFT studies, and ^1H, ^{19}F, $^{13}C\{^1H\}$ and $^{31}P\{^1H\}$ NMR Spectra. (PDF); optimized Cartesian coordinates in Å for structures related to Figure 3 (XYZ), structures related to Figure 5 (XYZ), structures related to Table 3 (XYZ) and method benchmark (XYZ). Animations of L_3 TS (GIF).

AUTHOR INFORMATION

Corresponding Author

* E-mail for R.T.B.: rbaker@uottawa.ca
* E-mail for C.E.: christian.ehm@unina.it

Author Contributions

The manuscript was written through contributions of all authors. / All authors have given approval to the final version of the manuscript.

ACKNOWLEDGMENT

We thank the NSERC and the Canada Research Chairs program for generous financial support and the University of Ottawa, Canada Foundation for Innovation and Ontario Ministry of Economic Development and Innovation for essential infrastructure. NOA gratefully acknowledges support from the province of Ontario, NSERC and the University of Ottawa (OGS and CGS-M/D).

REFERENCES

(1) New routes to fluoroalkenes: (a) Zheng, J.; Lin, J.-H.; Yu, L.-Y.; Wei, Y.; Zheng, X.; Xiao, J.-C. Cross-Coupling between Difluorocarbene and Carbene-Derived Intermediates Generated from Diazocompounds for the Synthesis of *gem*-Difluoroolefins. *Org. Lett.* **2015**, *17*, 6150-6153. (b) Zhang, W.; Wang, Y. Recent Advances in Carbon-Difluoroalkylation and -Difluoroolefination with Difluorocarbene. *Tetrahedron Lett.* **2018**, *59*, 1301-1308. (c) Okoromoba, O. E.; Han, J.; Hammond, G. B., Xu, B. C. Designer HF-Based Fluorination Reagent: Highly Regioselective Synthesis of Fluoroalkenes and *gem*-Difluoromethylene Compounds from Alkynes. *J. Am. Chem. Soc.* **2014**, *136*, 14381-14384. (d) Vandamme, M.; Paquin, J.-F. Eliminative Deoxofluorination Using XtalFluor-E: A One-Step Synthesis of Monofluoroalkenes from Cyclohexanone Derivatives. *Org. Lett.* **2017**, *19*, 3604-3607. (e) Yang, M.-H.; Matikonda, S. S.; Altman, R. A. Preparation of Fluoroalkenes via the Shapiro Reaction: Direct Access to Fluorinated Peptidomimetics. *Org. Lett.* **2013**, *15*, 3894-3897. (f) Sakaguchi, H.; Uetake, Y.; Ohashi, M.; Niwa, T.; Ogoshi, S.; Hosoya, T. Copper-Catalyzed Regioselective

Monodefluoroborylation of Polyfluoroalkenes en Route to Diverse Fluoroalkenes. *J. Am. Chem. Soc*. **2017**, *139*, 12855-12862. (g) Leclerc, M. C.; Gorelsky, S. I.; Gabidullin, B. M.; Korobkov, I.; Baker, R. T. Selective Activation of Fluoroalkenes with N-Heterocyclic Carbenes: Synthesis of N-Heterocyclic Fluoroalkenes and Polyfluoroalkenyl Imidazolium Salts. *Chem. Eur. J.* **2016**, *22*, 8063-8067.

(2) Uses of fluoroalkenes in the generation of fluoro-organics: (h) Andrella, N. O.; Sicard, A. J.; Gorelsky, S. I.; Korobkov, I.; Baker, R. T. A T-shaped Ni[κ^2-$(CF_2)_4$-] NHC complex: unusual C_{sp3}-F and M-C^F bond functionalization reactions. *Chem. Sci*. **2015**, *6*, 6392-6397. (i) Ritter, S. K Tetrafluoroethylene Is Good for More Than Just Teflon. *C&EN* **2015**, *93*(22), 28 (j) Ohashi, M.; Ogoshi, S. Transition Metal Mediated Transformations of Tetrafluoroethylene into Various Polyfluorinated Organic Compounds. *J. Synth. Org. Chem, Jpn.* **2016**, *74*, 1047-1057. (k) Ritter, S. K. A new edition of fluoroalkyl additions. *C&EN* **2017**, *95*(30), 9.

(3) (a) Ritter, S. K. Fluorochemicals go short. *C&EN* **2010**, *88*(5), 12. (b) Ritter, S. K. The Shrinking Case for Fluorochemicals. *C&EN* **2015**, *93*(28), 27. (c) Buck, R.C. Toxicology Data for Alternative "Short-Chain" Fluorinated Substances. In Toxicological Effects of Perfluoroalkyl and Polyfluoroalkyl Substances. Molecular and Integrative Toxicology, DeWitt, J., Eds.; Humana Press, Switzerland, 2015; pp. 451.(d) Mudumbi, J. B. N.; Ntwampe, S. K. O.; Matsha, T.; Mekuto, L.; Itoba-Tombo, E. F. Recent Developments in Polyfluoroalkyl Compounds Research: A Focus on Human/Environmental Health Impact, Suggested Substitutes and Removal Strategies. *Environ. Monit. Assess.* **2017**, *189*, 402.

(4) (a) Takahira, Y.; Morizawa, Y. Ruthenium-Catalyzed Oelfin Cross-Metathesis with Tetrafluoroethylene and Analogous Fluoroolefins. *J. Am. Chem. Soc.* **2015**, *137*, 7031-7034.

(5) Myhre, G.; Shindell, D.; Bréon, F.-M.; Collins, W.; Fuglestvedt, J.; Huang, J.; Koch, D.; Lamarque, J.-F.; Lee, D.; Mendoza, B.; Nakajima, T.; Robock, A.; Stephens, G.; Takemura, T.; Zhang, H. Anthropogenic and Natural Radiative Forcing. In Climate Change 2013: The Physical Science Basis. Contribution of Working Group I to the Fifth Assessment Report of the Intergovernmental Panel on Climate Change, Stocker, T.F.; Qin, D.; Plattner, G.-K.; Tignor, M.; Allen, S.K.; Boschung, J.; Nauels, A.; Xia, Y.; Bex, V.; Midgley, P.M., Eds.; Cambridge University Press, Cambridge, United Kingdom and New York, NY, USA, 2013.

(6) (a) Banks, R. E.; Smart, B. E.; Tatlow, J. C. Organofluorine Chemistry: Principles and Commercial Applications; Plenum: New York, 1994. (b) Chambers, R. D. Fluorine Chemistry at the Millennium; Elsevier: Amsterdam, 2000.

(7) *Examples of hydrodefluorination of fluoroarenes:* (a) Whittlesey, M. K.; Peris, E. Catalytic Hydrodefluorination with Late Transition Metal Complexes. *ACS Catal.* **2014**, *4*, 3152-3159. (b) Lv, H.; Cai. Y.-B.; Zhang, J.-L. Copper-catalyzed Hydrodefluorination of Fluoroarenes by Copper Hydride Intermediates. *Angew. Chem. Int. Ed.* **2013**, *52*, 3203-3207. (c) Cybulski, M. K.; McKay, D.; Macgregor, S. A.; Mahon, M. F.; Whittlesey, M. K. Room Temperature Regioselective Catalytic Hydrodefluorination of Fluoroarenes with *trans*-$[Ru(NHC)_4H_2]$ through a Concerted Nucleophilic Ru-H Attack Pathway. *Angew. Chem. Int. Ed.* **2017**, *56*, 1515-1519. (d) Kikushima, K.; Grellier, M.; Ohashi, M.; Ogoshi, S. Transition-Metal-Free Catalytic Hydrodefluorination of Polyfluoroarenes by Concerted Nucloephilic Aromatic Substitution with a Hydrosilicate. *Angew. Chem. Int. Ed.* **2017**, *56*, 16191-16196. (e) Krüger, J.; Leppkes, J.; Ehm, C.; Lentz, D. Competition of Nucloephilic Aromatic Substitution, *σ*-bond Metathesis, and *syn* Hydrometalation in Titanium (III)-Catylzed Hydrodefluorination of Arenes. *Chem. Asian J.* **2016**, *11*, 3062-3071. (f) Matsunami, A.; Kuwata, S.; Kayaki, Y. Hydrodefluorination of Fluoroarenes Using Hydrogen Transfer Catalysts with a Bifunctional Iridium/NH Moiety. *ACS Catal.* **2016**, *6*, 5181-5185.

(8) *Examples of hydrodefluorination of fluoroalkenes:* (a) Krüger, J.; Ehm, C.; Lentz, D. Improving Selectivity in Catalytic Hydrodefluorination by Limiting S_NV Reactivity. *Dalton Trans.* **2016**, *45*, 16789-16798. (b) Wu, J.; Xiao, J.; Dai, W.; Cao, S. Synthesis of Monofluoroalkenes Through Selective Hydrodefluorination of *gem*-Difluoroalkenes with Red-Al®. *RSC Adv.* **2015**, *5*, 34498-34501.

(9) Clot, E.; Mégret, C.; Kraft, B. M.; Eisenstein, O.; Jones, W. D. Defluorination of Perfluoropropene Using $Cp^*_2ZrH_2$ and Cp^*_2ZrHF: A Mechanism Investigation from a Joint Experimental-Theoretical Perspective. *J. Am Chem. Soc.* **2004**, *126*, 5647-5653.

(10) Kirkham, M. S.; Mahon, M. F.; Whittlesey, M. K. C-F Bond Activation of Perfluoroalkenes by Ruthenium Phosphine Hydride Complexes: X-ray Crystal Structures of *cis*-$Ru(dmpe)_2F(F\text{--}HF)$ and $[Ru(dcpe)_2H]^+[(CF_3)_2C{=}C(O)CF_2\text{-}CF_3]^-$. *Chem. Commun*, **2001**, *0*, 813-814. *Also see:* Noveski, D.; Braun. T.; Schulte, M.; Neumann, B.; Stammler, H.-G. C-F Activation and Hydrodefluorination of Fluorinated Alkenes at Rhodium. *Dalton Trans.* **2003**, 4075-4083.

(11) Vela, J.; Smith, M. J.; Yu, Y.; Ketterer, N. A.; Falschenriem, C. J.; Lachicotte, R. J.; Holland, P. L. Synthesis and Reactivity of Low-Coordinate Iron(II) Fluoride Complexes and Their Use in the Catalytic Hydrodefluorination of Fluorocarbons. *J. Am. Chem. Soc.* **2005**, *127*, 7857-7870.

(12) Kühnel, M. F.; Lentz, D. Titanium-Catalyzed C-F Activation of Fluoroalkenes. *Angew. Chem. Int. Ed.* **2010**, *49*, 2933-2936.

(13) a) Jaeger, A. D.; Ehm, C.; Lentz, D. Organocatalytic C-F Bond Activation with Alanes. *Chem. Eur. J.* **2018**, *24*, 6769-6777. b)*:* Schneider, H.; Hock, A.; Jaeger, A. D.; Lentz, D.; Radius, U. NHC Alane Adducts as Hydride Sources in the Hydrodefluorination of Fluoroaromatics and Fluoroolefins. *Eur. J. Inorg. Chem.* **2018**, *2018*, 4031-4043. c) Jaeger, A. D.; Walter, R.; Ehm, C.; Lentz, D., Gallium Hydrides and O/N-Donors as Tunable Systems in C−F Bond Activation. *Chem. Asian J.* **2018**, *13*, 2908-2915.

(14) (a) Hu, J.; Han, X.; Yuan, Y.; Shi, Z. Stereoselective Synthesis of Z-fluoroalkenes Through Copper-Catalyzed Hydrodefluorination of *gem*-Difluoroalkenes with Water. *Angew. Chem. Int. Ed.* **2017**, *56*, 13342-13346. (b) Kojima, R.; Kubota, K.; Ito, H. Stereodivergent Hydodefluorination of *gem*-Difluoroalkenes: Selective Synthesis of (*Z*)- and (*E*)-Monofluoroalkenes. *Chem. Commun.* **2017**, *53*, 10688-10691. (c) Andrella, N.O.; Liu, K.; Gabidullin, B.; Vasiliu, M.; Dixon, D. A.; Baker, R. T. Metal Heptafluoroisopropyl (M-hfip) Complexes for Use as hfip Transfer Agents. *Organometallics* **2018**, *37*, 422-432. (d) Baker, R. T., Andrella, N. O. Process for Preparation of Hydrofluoroalkenes

by Selective Catalytic Consecutive Hydrodefluorination. WO2018039794, March 8, 2018.

(15) Wilberg, K. B.; Murcko, M. A.; Laidig, K. E.; MacDougall, P. J. Origin of the Gauche Effect in Substituted Ethanes and Ethenes. *J. Phys. Chem.*, **1990**, *94*, 6956-6959.

(16) (a) Burton, D. J. Fluorinated Ylides and Related Compounds. *Chem. Rev.*, **1996**, *96*, 1641-1716. b) Leclerc, M. C.; Da Gama, J. G.; Gabidullin, B. M.; Baker, R. T. A Closer Look at the Reactivity Between N-Heterocyclic Carbenes and Fluoroalkenes. *J. Fluorine Chem.*, **2017**, *203*, 81-89.

(17) a) Jordan, A. J.; Wyss, C. M.; Bacsa, J.; Sadighi, J. P. Synthesis and Reactivity of New Copper(I) Hydride Dimers. *Organometallics*, **2016**, *35*, 613-616. b) Frey, G. D.; Donnadieu, B.; Solelhavoup, M.; Bertrand, G. Synthesis of a Room-Temperature-Stable Dimeric Copper(I) Hydride. *Chem. Asian J.*, **2011**, *6*, 402-406. c) Jordan, A. J.; Lalic, G.; Sadighi, J. P. Coinage Metal Hydrides: Synthesis, Characterization, and Reactivity. *Chem. Rev.*, **2016**, *116*, 8318-8372.

(18) (a) Li, L.; Ni, C.; Xie, Q.; Hu, M.; Wang. F.; Hu, J. $TMSCF_3$ as a Convenient Source of CF_2=CF_2 for Pentafluoroethylation, (Aryloxy)tetrafluoroethylation, and Tetrafluoroethylation. *Angew. Chem. Int. Ed.* **2017**, *56*, 9971-9975. (b) Ohashi, M.; Ishida, N.; Ando, K.; Hashimoto, Y.; Shigaki, A.; Kikushima, K.; Ogoshi, S. Cu^{I}- Catalyzed Pentafluoroethylation of Aryl Iodides in the Presence of Tetrafluoroethylene and Cesium Fluoride: Determining the Route to the Key Pentafluoroethyl Cu^{I} Intermediate. *Chem. Eur. J.* **2018**, *24*, 9794-9798.

(19) (a) Romero, E. A.; Olsen, P. M.; Jazzar, R.; Soleilhavoup, M.; Gembicky, M.; Bertrand, G., Spectroscopic Evidence for a Monomeric Copper(I) Hydride and Crystallographic Characterization of a Monomeric Silver(I) Hydride. *Angew. Chem. Int. Ed.* **2017**, *56*, 4024-4027. (b) Goeden, G. V.; Huffman, J. C.; Caulton, K. G., A Cu-(μ-H) Bond Can Be Stronger Than an Intramolecular P-C Bond. Synthesis and Structure of Cu-$(\mu\text{-H})_2[\eta^2\text{-}CH_3C(CH_2PPh_2)_3]_2$. *Inorg. Chem.* **1986**, *25*, 2484-2485. (c) Mankad, N. P.; Laitar, D. S.; Sadighi, J. P., Synthesis, Structure, and Alkyne Reactivity of a Dimeric (Carbene)copper(I) Hydride. *Organometallics* **2004**, *23*, 3369-3371. (c) Zall, C. M.; Linehan, J. C.; Appel, A. M., Triphosphine-Ligated Copper Hydrides for CO_2 Hydrogenation: Structure, Reactivity, and Thermodynamic Studies. *J. Am. Chem. Soc.* **2016**, *138*, 9968-9977. (d) Dhayal, R. S.: van Zyl, W. E.; Liu, C. W., Copper Hydride Clusters in Energy Storage and Conversion. *Dalton Trans.* **2019**, *48*, 3531-3538.

(20) Chen, J.-X.; Daeuble, J. F.; Brestensky, D. M.; Stryker, J. M., Highly Chemoselective Catalytic Hydrogenation of Unsaturated Ketones and Aldehydes to Unsaturated Alcohols Using Phosphine-Stabilized Copper(I) Hydride Complexes. *Tetrahedron* **2000**, *56*, 2153-2166.

(21) Issenhuth, J.-T.; Notter, F.-P.; Dagorne, S.; Dedieu, A.; Bellemin-Laponnaz, S., Mechanistic Studies on the Copper-Catalyzed Hydrosilylation of Ketones. *Eur. J. Inorg. Chem.* **2010**, *2010*, 529-541.

(22) Kuehnel, M. F.; Lentz, D.; Braun, T., Synthesis of Fluorinated Building Blocks by Transition-Metal-Mediated Hydrodefluorination Reactions. *Angew. Chem. Int. Ed.* **2013**, *52*, 3328-3348.

(23) Aizenberg, M.; Milstein, D., Homogeneous Rhodium Complex-Catalyzed Hydrogenolysis of C-F bonds. *J. Am. Chem. Soc.* **1995**, *117*, 8674-8675.

(24) Hintermann, S.; Pregosin, P. S.; Rüegger, H.; Clark, H. C., Electron Transfer Reactions Involving *trans*-$[PtH_2(PCy_3)_2]$ and Fluorinated Benzonitriles. *J. Organomet. Chem.* **1992**, *435*, 225-234.

(25) Kraft, B. M.; Lachicotte, R. J.; Jones, W. D., Aliphatic and Aromatic Carbon−Fluorine Bond Activation with $Cp^*_2ZrH_2$: Mechanisms of Hydrodefluorination. *J. Am. Chem. Soc.* **2001**, *123*, 10973-10979.

(26) Lu, H.; Cai, Y.-B.; Zhang, J.-L., Copper-Catalyzed Hydrodefluorination of Fluoroarenes by Copper Hydride Intermediates. *Angew. Chem. Int. Ed.* **2013**, *52*, 3203-3207

(27) Panetier, J. A.; Macgregor, S. A.; Whittlesey, M. K., Catalytic Hydrodefluorination of Pentafluorobenzene by $[Ru(NHC)(PPh_3)_2(CO)H_2]$: A Nucleophilic Attack by a Metal-Bound Hydride Ligand Explains an Unusual ortho-Regioselectivity. *Angew. Chem. Int. Ed.* **2011**, *50*, 2783-2786

(28) D., J. A.; Christian, E.; Dieter, L., Organocatalytic C−F Bond Activation with Alanes. *Chem. Eur. J.* **2018**, *24*, 6769-6777.

(29) Ehm, C.; Krüger, J.; Lentz, D., How a Thermally Unstable Metal Hydrido Complex Can Yield High Catalytic Activity Even at Elevated Temperatures. *Chem. Eur. J.* **2016**, *22*, 9305-9310

(30) Luo, Y. R., *Comprehensive Handbook of Chemical Bond Energies*. CRC Press: Boca Rayton, FL, 2007.

(31) Ehm, C.; Lentz, D., Partially Fluorinated Butatrienes: A Coupled Cluster Study. *J. Phys. Chem. A* **2010**, *114*, 3609-3614.

(32) Ehm, C.; Lentz, D., Cyclic Dimers of Tetrafluorobutatriene. *Theor. Chem. Acc.* **2011**, *129*, 507-515.

(33) Wiberg, K. B., Application of the Pople-Santry-Segal CNDO Method to the Cyclopropylcarbinyl and Cyclobutyl Cation and to Bicyclobutane. *Tetrahedron* **1968**, *24*, 1083-1096.

(34) Glendening, E. D.; Badenhoop, J. K.; Reed, A. E.; Carpenter, J. E.; Bohmann, J. A.; Morales, C. M.; Weinhold, F. *NBO 5.0*, Theoretical Chemistry Institute, University of Wisconsin, Madison, WI, URL: http://nbo6.chem.wisc.edu/.

(35) Tolman, C. A., Steric Effects of Phosphorus Ligands in Organometallic Chemistry and Homogeneous Catalysis. *Chem. Rev.* **1977**, *77*, 313-348

(36) See for example: Walther, D.; Liesicke, S.; Böttcher, L.; Fischer, R.; Görls, H.; Vaughan, G., Metal Complexes with 2,3-Bis(diphenylphosphino)-1,4-diazadiene Ligands: Synthesis, Structures, and an Intramolecular Metal-Mediated [4+2] Cycloaddtion Employing a Benzene Ring as a Dienophile. *Inorg. Chem.* **2003**, *42*, 625-632.

(37) Craig, N. C.; Entemann, E. A., Thermodynamics of *cis-trans* Isomerizations. The 1,2-Difluoroethylenes. *J. Am. Chem. Soc.* **1961**, *83*, 3047-3050

(38) Iwashita, A.; Chan, M. C. W.; Makio, H.; Fujita, T., Attractive Interactions in Olefin Polymerization Mediated by Post-Metallocene Catalysts with Fluorine-Containing Ancillary Ligands. *Catal. Sci. Technol.* **2014**, *4*, 599-610.

(39) Talarico, G.; Busico, V.; Cavallo, L., "Living" Propene Polymerization with Bis(phenoxyimine) Group 4 Metal Catalysts: New Strategies and Old Concepts. *Organometallics* **2004**, *23*, 5989-5993.

(40) Reed, A. E.; Curtiss, L. A.; Weinhold, F., Intermolecular Interactions From a Natural Bond Orbital, Donor-Acceptor Viewpoint. *Chem Rev.* **1988**, *88*, 899-926.

(41) Minenkov, Y.; Occhipinti, G.; Jensen, V. R., Metal−Phosphine Bond Strengths of the Transition Metals: A

Challenge for DFT†. *J. Phys. Chem. A* **2009**, *113*, 11833-11844.

(42) Falivene, L.; Credendino, R.; Poater, A.; Petta, A.; Serra, L.; Oliva, R.; Scarano, V.; Cavallo, L., SambVca 2. A Web Tool for Analyzing Catalytic Pockets with Topographic Steric Maps. *Organometallics* **2016**, *35*, 2286-2293.

(43) Banerjee, D.; Ghosh, A.; Chattopadhyay, S.; Ghosh, P.; Chaudhuri, R. K., Revisiting the '*Cis*-Effect' in 1,2-difluoro Derivatives of Ethylene and Diazene Using Ab Initio Multireference Methods. *Mol. Phys.* **2014**, *112*, 3206-3224.

(44) Bingham, R. C., The Stereochemical Consequences of Electron Delocalization in Extended π- Systems. An interpretation of the *Cis* Effect Exhibited by 1,2-Disubstituted Ethylenes and Related Phenomena. *J. Am. Chem. Soc.* **1976**, *98* (2), 535-540.

(45) Wiberg, K. B.; Hadad, C. M.; Breneman, C. M.; Laidig, K. E.; Murcko, M. A.; Lepage, T. J., The Response of Electrons to Structural Changes. *Science* **1991**, *252*, 1266.

(46) Wiberg, K. B.; Murcko, M. A.; Laidig, K. E.; MacDougall, P. J., Origin of the Gauche Effect in Substituted Ethanes and Ethenes. *J. Phys. Chem.* **1990**, *94*, 6956-6959.

(47) Ditchfield, R.; Ellis, P. D., ^{13}C NMR Chemical Shifts for Fluoroethylenes and Fluoroacetylene. *Chem. Phys. Lett.* **1972**, *17*, 342-344.

(48) Yamamoto, T.; Tomoda, S., On the Origin of *cis*-Effect in 1,2-Difluoroethene. *Chem. Lett.* **1997**, *26*, 1069-1070.

(49) Cremer, D., The Role of Correlation in Calculations on 1,2-Difluoroethylenes. The *cis-trans* Energy Difference. *Chem. Phys. Lett.* **1981**, *81*, 481-485.

(50) Feller, D.; Craig, N. C.; Groner, P.; McKean, D. C., Ab Initio Coupled Cluster Determination of the Equilibrium Structures of *cis*- and *trans*-1,2-Difluoroethylene and 1,1-Difluoroethylene. *J. Phys. Chem. A.* **2011**, *115*, 94-98.

(51) Farcasiu, D., The Use and Misuse of the Hammond Postulate. *J. Chem. Educ.* **1975,** *52*, 76.

(52) Hammond, G. S., A Correlation of Reaction Rates. *J. Am. Chem. Soc.* **1955**, *77*, 334-338.

(53) IRC scans show that F-elimination proceeds first towards the electron poor P, then to the Cu. In the presence of silanes, an OR group could therefore be abstracted, which would lead to catalyst decomposition.

(54) With the isolated complex preliminary reactivity was explored. Cross-coupling of the tetrafluoroethyl complex **7a** with iodobenzene (5 eq.) in the presence of 10 mol% of [(1,3-bis(2,4,6-trimethylphenyl)-4,5-dihydroimidazol-2-ylidene) copper(I) chloride] (80 % yield, determined by ^{19}F NMR) could be achieved. This represents a new route for the introduction of the CF_2CF_2H moiety to organic compounds. The use of **7b** under the same reaction conditions proved ineffective. Further investigation of this reaction is beyond the scope of this publication and will be reported in due course.

(55) Bantreil, X.; Nolan, S. P. Synthesis of N-Heterocyclic Carbene Ligands and Derived Ruthenium Olefin Metathesis Catalysts. *Nat. Protoc.* 2011, 6, 69-77

(56) Lee, D.-W.; Yun, J. Direct Synthesis of Stryker's Reagent from a Cu(II) Salt. *Tetrahedron Lett.* **2005**, *46*, 2037-2039.

(57) Hunadi, R. J.; Baum, K. Tetrafluoroethylene: A Convenient Laboratory Preparation. *Synthesis* **1982**, *39*, 454.

(58) Hercules, D. A.; Parrish, C. A.; Sayler, T. S.; Tice, T. K.; Williams, S. M.; Lowery, L. E.; Brady, M. E.; Coward, R. B.; Murphy, J. A.; Hey, T. A.; Scavuzzo, A. R.; Rummler, L. M.; Burns, E. G.; Matsnev, A. J.; Fernandez, R. E.; McMillen, C. D.; Thrasher, J. S. Preparation of Tetrafluoroethylene from the Pyrolysis of Pentafluoropropionate Salts. *J. Fluorine Chem.*, **2017**, *196*, 107-116.

(59) (a) Koroniak, H.; Palmer, K. W.; Dolbier, W. R.; Zhang, H.^{19}F NMR Properties of Some Trifluorovinyl- and Pentafluoropropenyl-Substituted Aromatics. *Magn. Reson. Chem.* **1993**, *31*, 748-751. (b) Burton, D. J.; Spawn, T. W.; Heinze, P. L.; Bailey, A. R.; Shin-Ya, S. Preparation of *E*-1,2,3,3,3-Pentafluoropropene, *Z*-1,2,3,3,3-Pentafluoropropene and *E*-1-Iodopentafluoropropene. *J. Fluorine Chem.* **1989**, *44*, 167-174.

(60) Banks, R. E., Barlow, M. G., Nickkho-Amiry, M. Preparation of 2,3,3,3-Tetrafluoropropene from Trifluoroacetylacetone and Sulphur Tetrafluoride. *J. Fluorine Chem.* **1997**, *82*, 171-174.

(61) Meißner, G., Kretschmar, K., Braun, T., Kemnitz, E. Consecutive Transformations of Tetrafluoropropenes: Hydrogermylation and Catalytic C-F Activation Steps at a Lewis Acidic Aluminium Fluoride. *Angew. Chem. Int. Ed.* **2017**, *56*, 16338-16341.

(62) Emsley, J. W., Phillips, L. Fluorine Chemical Shifts. *Prog. Nucl. Magn. Reson. Spectrosc.* **1971,** *7*, 1-520.

(63) Brey, W. S. ^{19}F and ^{13}C Spectra of Fluorinated and Partially Fluorinated Vinyl Alkyl Ethers. *J. Fluorine Chem.* **2005**, *126*, 389-399.

(64) Kučnirová, K.; Šimůnek, O.; Rybáčkoá, M.; Kvíčala, J. Structural Assignment of Fluorocyclobutenes by ^{19}F NMR Spectroscopy – Comparison of Calculated ^{19}F NMR Shielding Constants with Experimental ^{19}F NMR Shifts. *Eur. J. Org. Chem.* **2018**, *2018*, 3867-3874.

(65) Snegirev, V. F.; Makarov, K. N.; Zabolotskikh, V. F.; Sorokina, M. G.; Knunyants, I. L. Catalytic and Hydride Reduction of Hexafluoropropylene Dimers. *Russ. Chem. Bull.* **1983**, *32*, 2489-2494.

(66) (a) Edwards, M. L.; Stemerick, D. M.; Jarvi, E. T.; Matthews, D. P.; McCarthy, J. R. Difluoromethyldiphenylphosphine Oxide. A New Reagent for Conversion of Carbonyl Compounds to 1,1-Difluoroolefins. *Tetrahedron Lett.* **1990**, *31*, 5571-5574. (b) Tian, H.; Shimakoshi, H.; Imamura, K.; Shiota, Y.; Yoshizawa, K.; Hisaeda, Y. Photocatalytic Alkene Reduction by a B_{12}-TiO_2 Hybrid Catalyst Coupled with C-F Bond Cleavage for *gem*-Difluoroolefin Synthesis. *Chem. Commun*. **2017**, *53*, 9478-9481.

(67) Gaussian 09 Revision B.1; for the full citation see the Supporting Information.

(68) J. Baker, 2.4 ed., Parallel Quantum Solutions, Fayetteville, AR, 2001.

(69) Baker, J., An Algorithm for the Location of Transition States. *J. Comput. Chem.* **1986**, *7*, 385-395.

(70) Budzelaar, P. H. M., Geometry Optimization Using Generalized, Chemically Meaningful Constraints. *J. Comput. Chem.* **2007**, *28*, 2226-2236.

(71) Ehm, C.; Budzelaar, P. H. M.; Busico, V., Calculating Accurate Barriers for Olefin Insertion and Related Reactions. *J. Organomet. Chem.* **2015**, *775*, 39-49.

(72) Tao, J.; Perdew, J. P.; Staroverov, V. N.; Scuseria, G. E., Climbing the Density Functional Ladder: Nonempirical Meta-Generalized Gradient Approximation Designed for Molecules and Solids. *Phys. Rev. Lett.* **2003**, *91*, 146401.

(73) Balabanov, N. B.; Peterson, K. A., Systematically Convergent Basis Sets for Transition Metals. I. All-electron

Correlation Consistent Basis Sets for the 3d Elements Sc–Zn. *J. Chem. Phys.* **2005**, *123*, 064107.

(74) Balabanov, N. B.; Peterson, K. A., Basis Set Limit Electronic Excitation Energies, Ionization Potentials, and Electron Affinities for the 3d Transition Metal Atoms: Coupled Cluster and Multireference Methods. *J. Chem. Phys.* **2006**, *125*, 074110.

(75) Schuchardt, K. L.; Didier, B. T.; Elsethagen, T.; Sun, L. S.; Gurumoorthi, V.; Chase, J.; Li, J.; Windus, T. L., Basis Set Exchange: A Community Database for Computational Sciences. *J. Chem. Inf. Model* **2007**, *47*, 1045-1052

(76) Whitten, J. L., Coulombic Potential Energy Integrals and Approximations. *J. Chem. Phys.* **1973**, *58*, 4496.

(77) Baerends, E. J.; Ellis, D. E.; Ros, P., Self-Consistent Molecular Hartree—Fock—Slater Calculations I. The Computational Procedure. *Chem. Phys.* **1973**, *2*, 41-51

(78) Feyereisen, M.; Fitzgerald, G.; Komornicki, A., Use of Approximate Integrals in *Ab Initio* Theory. An Application in MP2 Energy Calculations. *Chem. Phys. Lett.* **1993**, *208*, 359-363.

(79) Vahtras, O.; Almlöf, J.; Feyereisen, M. W., Integral Approximations for LCAO-SCF Calculations. *Chem. Phys. Lett.* **1993**, *213*, 514-518.

(80) Tomasi, J., Thirty Years of Continuum Solvation Chemistry: A Review and Prospects for the Near Future. *Theor. Chem. Acc.* **2004**, *112*, 184-203.

(81) The Berny algorithm was never fully published, see the Gaussian documentation for details.

(82) Tao, J. M.; Perdew, J. P.; Staroverov, V. N.; Scuseria, G. E., Climbing the Density Functional Ladder: Nonempirical Meta-Generalized Gradient Approximation Designed for Molecules and Solids. *Phys. Rev. Lett.* **2003**, *91*

(83) Grimme, S., Density Functional Theory with London Dispersion Corrections. *Wiley Interdiscip. Rev. Comput. Mol. Sci.* **2011**, *1*, 211-228.

(84) Grimme, S.; Ehrlich, S.; Goerigk, L., Effect of the Damping Function in Dispersion Corrected Density Functional Theory. *J. Comput. Chem.* **2011**, *32*, 1456-1465.

(85) Tobisch, S.; Ziegler, T., Catalytic Oligomerization of Ethylene to Higher Linear α-Olefins Promoted by the Cationic Group 4 $[(\eta^5\text{-Cp-}(CMe_2\text{-bridge)-Ph})M^{II}(\text{ethylene})_2]^+$ (M = Ti, Zr, Hf) Active Catalysts: A Density Functional Investigation of the Influence of the Metal on the Catalytic Activity and Selectivity. *J. Am. Chem. Soc.* **2004**, *126*, 9059-9071.

(86) Dunlop-Brière, A. F.; Budzelaar, P. H. M.; Baird, M. C., α- and β-Agostic Alkyl–Titanocene Complexes. *Organometallics* **2012**, *31*, 1591-1594.

(87) Raucoules, R.; de Bruin, T.; Raybaud, P.; Adamo, C., Theoretical Unraveling of Selective 1-Butene Oligomerization Catalyzed by Iron−Bis(arylimino)pyridine. *Organometallics* **2009**, *28*, 5358-5367.

(88) Glendening, E. D.; Landis, C. R.; Weinhold, F., Natural Bond Orbital Methods. *Wiley. Interdiscip. Rev. Comput. Mol. Sci.* **2012**, *2*, 1–42.

(89) Grimme, S., Semiempirical GGA-type Density Functional Constructed with a Long-Range Dispersion Correction. *J. Comput. Chem.* **2006**, *27*, 1787-1799.

(90) Miyawaki, J.; Sugawara, K.-I., ZEKE Photoelectron Spectroscopy of the Silver- and Copper-ammonia Complexes. *J. Chem. Phys.* 2003, 119, 6539-6545.

(91) Meyer, F.; Chen, Y.-M.; Armentrout, P. B., Sequential Bond Energies of $Cu(CO)_x^+$ and $Ag(CO)_x^+$ (x = 1-4). *J. Am. Chem. Soc.* **1995**, *117*, 4071-4081.

(92) a) Sievers, M. R.; Jarvis, L. M.; Armentrout, P. B., Transition-Metal Ethene Bonds: Thermochemistry of $M^+(C_2H_4)_n$ (M = Ti-Cu, n = 1 and 2) Complexes. *J. Am. Chem. Soc.* **1998**, *120*, 1891-1899. b) Hertwig, R. H.; Koch, W.; Schröder, D.; Schwarz, H., A Comparative Computational Study of Cationic Coinage Metal-Ethylene Complexes $(C_2H_4)M^+$ (M = Cu, Ag, and Au). *J. Phys. Chem.* **1996**, *100*, 12253-12260.

(93) Vitale, G.; Valina, A. B.; Huang, H.; Amunugama, R.; Rodgeers, M. T., Solvation of Copper Ions by Acetonitrile. Structures and Sequential Binding Energies of $Cu^+(CH_3CN)_x$, x = 1-5, from Collision-Induced Dissociation and Theoretical Studies. *J. Phys. Chem.* **2001**, *105*, 11351-11364.

SYNOPSIS TOC (Word Style "SN_Synopsis_TOC"). If you are submitting your paper to a journal that requires a synopsis graphic and/or synopsis paragraph, see the Instructions for Authors on the journal's homepage for a description of what needs to be provided and for the size requirements of the artwork.

Authors are required to submit a graphic entry for the Table of Contents (TOC) that, in conjunction with the manuscript title, should give the reader a representative idea of one of the following: A key structure, reaction, equation, concept, or theorem, etc., that is discussed in the manuscript. Consult the journal's Instructions for Authors for TOC graphic specifications.